High-pressure structures and phase transformations in elemental metals

Malcolm I. McMahon and Richard J. Nelmes

Received 6th July 2006
First published as an Advance Article on the web 30th August 2006
DOI: 10.1039/b517777b

At ambient conditions the great majority of the metallic elements have simple crystal structures, such as face-centred or body-centred cubic, or hexagonal close-packed. However, when subjected to very high pressures, many of the same elements undergo phase transitions to low-symmetry and surprisingly complex structures, an increasing number of which are being found to be incommensurate. The present *critical review* describes the high-pressure behaviour of each of the group 1 to 16 metallic elements in detail, summarising previous work and giving the best present understanding of the structures and transitions at ambient temperature. The principal results and emerging systematics are then summarised and discussed.

1. Introduction

Many new elemental structures have been discovered in the last 10 years. In this review, we focus on those elements that are metallic or semi-metallic under ambient conditions as it is in these that the most new structures and striking structural complexity have been found. Amongst the elements that we will cover—as highlighted in Fig. 1—particularly remarkable increases in complexity under pressure have been found so far in groups 1, 2, 3, 13, 15 and 16. We first briefly overview what is known of the elements as a whole, and outline the experimental advances that have revealed so many new structures in recent years.

The elements are the most fundamental materials and their high-pressure behaviour has attracted the attention of many researchers since the pioneering work of Bridgman in the first half of the 20th century.[1] At ambient conditions, the majority of the solid, non-molecular elements adopt very simple high-symmetry structures, many of which are body-centred cubic (*bcc*), face-centred cubic (*fcc*), cubic close-packed or hexagonal close-packed (*hcp*).[2] It might be expected that these would merely compress under high compression and that those elements whose structures were not yet close-packed or *bcc* would become so. However, differences in the density dependence of electronic energy levels can change the nature of the bonding such that there may be structural transitions to phases with lower symmetry and less close packing than found at ambient pressure. Changes of structure and electronic energy levels can also give rise to dramatic changes in physical properties. Elements that are insulators at ambient pressure exhibit structural phase transitions accompanied by metallization and the onset of superconductivity,[3] and even elements such as boron,[4] oxygen[5] and sulfur[6] have been observed to become superconducting metals at very high pressures. Indeed, a recent review of pressure-induced superconductivity in the elements[3] reveals that the number of known elemental superconductors has been increased by over 70% by high-pressure studies. Applying pressure can also induce transitions from

SUPA, School of Physics and Centre for Science at Extreme Conditions, The University of Edinburgh, Mayfield Road, Edinburgh, EH9 3JZ, U.K.

Malcolm McMahon

Malcolm McMahon was born in Scotland, and obtained his BSc degree in Physics from the University of Edinburgh in 1987, and his PhD, also from the University of Edinburgh, in 1991. After completing his PhD he was based at the Synchrotron Radiation Source in the UK, where he worked on the development of angle-dispersive diffraction techniques for studying systems at high pressures. He was a Royal Society University Research Fellow at the Universities of Liverpool and Edinburgh from 1996–2003, after which he took up his present position as Reader at the University of Edinburgh. His research interests cover all aspects of high-pressure structural physics.

Richard Nelmes

Richard Nelmes graduated from the University of Cambridge, and then took his PhD in Physics at the University of Edinburgh under the supervision of William Cochran, with whom he did postdoctoral work until appointment as a Lecturer in 1976. After nearly 20 years of research on ferroelectric structures and phase transitions, he used a Senior Fellowship from SERC (now EPSRC) to move into a specialisation in high-pressure structural physics, and his group at Edinburgh have developed leading techniques for both neutron and X-ray synchrotron diffraction. He is now Chairman of the recently established Centre for Science at Extreme Conditions in Edinburgh.

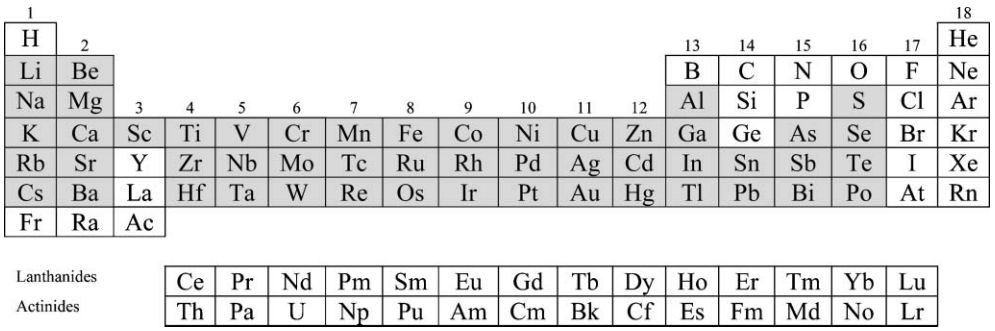

Fig. 1 The periodic table showing shaded the elements covered in this review. Groups are numbered at the top of each column.

molecular to non-molecular structural forms,[7] convert graphite into diamond,[8] and polymerise simple molecules such as N_2.[9] And the conversion of gaseous molecular hydrogen to a monatomic metallic superconductor is, for many, the ''holy grail'' of high-pressure physics.[10]

Reviews of what was known about the high-pressure behaviour of the elements as of 1976 and 1991 can be found in Refs 11 and 12, respectively. The work described therein established general structural trends within the different groups of the periodic table, in particular the fact that the heavier (higher-Z) members of a group tend to follow the same general sequence of structural changes as the lighter members but at lower pressures—and this still broadly remains the case. The extensive information then available, particularly for elements like silicon, also proved important in testing the first *ab initio* computational studies of structural density dependence in the 1980's.[13,14] The majority of the high-pressure phases successfully studied at that time involved transitions to simple, high-symmetry (cubic, tetragonal or hexagonal) structures, although there were already known to be a significant number that appeared more complex and resisted attempts at solution.[12] There were also several high-pressure phases, such as Bi-III,[15] whose published structures did not provide as good a fit as might be expected to the data.

The problem in solving complex structures at high pressure arose through two principal difficulties: first, the perceived necessity of using powder-diffraction methods, because single-crystals did not typically survive the strongly first-order transitions observed on compression; and secondly the use of energy-dispersive diffraction techniques which utilised intense polychromatic X-ray radiation to overcome the weak signal given by the small volume of samples at very high pressures in typical pressure cells. These techniques were highly successful in enabling the high-pressure behaviour of many of the elements to be followed to above 100 GPa and their phase diagrams to be mapped over wide ranges of pressure and temperature,[12] but the modest resolution and unreliable peak intensities of energy-dispersive powder diffraction data prevented the solution of more complex structures. The introduction of image-plate area detectors in Japan in the early 1990's opened up a move to angle-dispersive powder-diffraction methods[16] which were then developed at the SRS synchrotron in the UK into powerful techniques that exploit both the higher resolution of angle-dispersive methods and also the potential of an area detector to give data with better powder averaging.[17] Our developments at SRS introduced the use of pressure cells with wide-angle conical apertures, full 2-D data collection and integration of the 2-D powder patterns,[17] which resulted in unprecedented sensitivity to the weak diffraction features that reveal reduced symmetries. The integration of full 2-D patterns also provided much more accurate peak intensities, making full-profile (Rietveld) refinement of high-pressure phases routinely possible for the first time. This approach has since revolutionised high-pressure structural studies using powder diffraction methods and led to much new work on the elements.

An unexpected outcome of the move to these optimised angle-dispersive methods was the discovery of structures that were still too complex to solve! It became clear that the level of structural complexity being uncovered was such that the intrinsic 1-D nature of powder diffraction data, and the consequent peak overlap, was becoming the limiting factor in some cases. Our group therefore started to develop the use of single-crystal methods. One of the factors that limited the effectiveness of powder methods was the tendency of complex phases with one or more large unit-cell dimensions to form quite large crystallites, and thus give 'spotty' powder patterns. It often proved possible to exploit this tendency to recrystallise and use it to grow a small number of crystallites from which quasi-single-crystal data could be obtained by collecting data on a 2-D CCD detector and determining the orientations of the various crystallites.[18] In one case, a structure was solved from a sample made up of seven slightly misaligned crystallites.[19] And it also proved possible sometimes to coax quasi-single crystal samples through first-order phase transitions that had been thought to prevent the use of single-crystal methods.[20] In these ways, single-crystal diffraction techniques have been successfully applied to a growing number of studies of high-pressure phases previously thought to be accessible only to powder methods.

Powder and single-crystal diffraction studies of the past decade, using these refined methods, have revealed a wealth of previously unidentified phases, resolved previous ambiguities in the reported structures, and uncovered a number of wholly new complex structure types previously unknown in the elements. These have included remarkable surprises like composite incommensurate phases, and *fcc* Cs transforming under pressure into a complex modulated layer structure with 84 atoms in the unit cell.[18] At the same time, there have been advances in other experimental techniques, such as

spectroscopy and transport-property measurements, and developments in computational methods, particularly in the availability of greater computer power allowing the use of *ab initio* density functional methods.[21] Tonkov and Ponyatovsky[22] have recently published an extensive overview of the current state of the wider experimental knowledge about the elements under pressure, including also reference to key calculations.

Our review focuses on structural aspects, and provides details of all the known high-pressure transitions and phases in the elements that are metallic or semi-metallic at ambient pressure, as explained above. However, we have omitted the lanthanides and actinides: their electronic configurations mean that their high-pressure behaviour is generally unique to those groups of elements and, given this and their extensive literature, they merit a separate review. Two exceptions are the inclusion of the ambient-pressure insulator S for comparison with Se and Te, and the inclusion of the actinide U as it has an incommensurate phase to be compared with those in the group 16 elements. We also focus on structures and transitions as found at room temperature, where almost all detailed structure determinations have so far been made. Much is known about the *P*–*T* phase diagrams of the elements from a wealth of density, electrical, thermal, spectroscopic and (energy-dispersive) diffraction measurements, as reviewed by Tonkov and Ponyatovsky,[22] and there is a clear need for high-resolution structural studies at high and low temperatures, but few have so far been carried out. The lack of high-temperature data at high pressure means that there is also little in detail yet known about the high-pressure structures of the liquid phases. However, the same angle-dispersive techniques used for powder diffraction are being used increasingly to carry out such,[23–26] and melting curves are being determined to extremes of pressure and temperature.[27] A particular driving force behind this work is to understand Fe at Earth core conditions.[28]

In the next section, we provide a summary and description of the key structures to be discussed in the rest of the review. In Section 3, we review groups 1 to 16 in turn, summarising previous work and giving the best present understanding of the room-temperature structures and transitions. The principal results and emerging systematics are summarised and discussed in Section 4.

2. Structures

The key new structures in the metallic and semi-metallic elements fall naturally into 4 categories: incommensurate composite structures, incommensurately modulated structures, modulated layer structures, and other complex structures. In this section, we provide a detailed description of all of these, and the form they take in the phases in which they occur. We group the 'other complex structures' together with other non-simple-close-packed structures in Section 2.4, and do not include the commonly occurring body-centred cubic (*bcc*), face-centred cubic (*fcc*) and hexagonal close-packed (*hcp*) structures. We refer the reader to the excellent descriptions given by Donohue[2] for the details of some of the more long-established and well known ambient-pressure structures

2.1 Incommensurate composite structures

Incommensurate composite structures comprise two interpenetrating components, a 'host' and a 'guest', which are incommensurate with each other along one or more axes. This structure type is well known in organic, inorganic, organometallic and mineral compounds (see Ref. 29 for examples) but, given its two-component nature, is very unexpected in elements and is not known in any of them at ambient pressure. However, after it was first found above 12 GPa in barium in 1999,[30] it has been observed in high-pressure phases of seven other elements,[31–37] and has thus emerged as an important elemental form. The first solution of a structure of this wholly unexpected kind could have been achieved only with single-crystal methods, as the incommensurate nature of the structure meant that standard indexing methods would have been unsuccessful. Ba-IV also gives strongly textured, ''spotty'' diffraction patterns[30] and it was this that we utilised to grow a high-quality single crystal of the phase.

The composite structure of Ba-IVa, as viewed in projection down the *c* axis, is shown in Fig. 2a. The 8-atom host structure has space group *I*4/*mcm*, with atoms on the 8*h* site at (0.1486(1), $x + \frac{1}{2}$,0) and tetragonal lattice parameters $a_H = b_H = 8.4207(13)$ Å and $c_H = 4.7369(4)$ Å at 12.1 GPa.[30,37] This host framework has octagonal channels along the *c*-axis, contained within which are linear chains of atoms that make up the guest structure, which is *C*-face centred monoclinic, space group *C*2/*m* (Fig. 2b), with $a_G = 8.4623(35)$ Å, $b_G = b_H$, $c_G = 3.4269(7)$ Å, and $\beta_G = 96.151(9)^\circ$ at 12.1 GPa.[30,37] The host and guest structures are commensurate with each other in the *a*–*b* plane, but they are incommensurate with each other along their common *c* axis. Ba-IVa also exhibits a second, coexisting guest structure, which is *C*-face centred tetragonal (Fig. 2c), space group *C*4/*mmm* with $a_G = a_H = 8.4207(13)$ Å and $c_G = 3.4117(5)$ Å at 12.1 GPa, but this appears not to be an equilibrium form.[30,37]

Structures with the same 8-atom host framework have been found in Sr, Sc, As, Sb and Bi[31,34–37] and, with a small distortion to monoclinic symmetry, in As and Sb.[34,35] Similarities with Ba-IV suggested the same structural type, and the details were solved from powder data, although in the case of Bi a quasi-single-crystal sample was used to show the

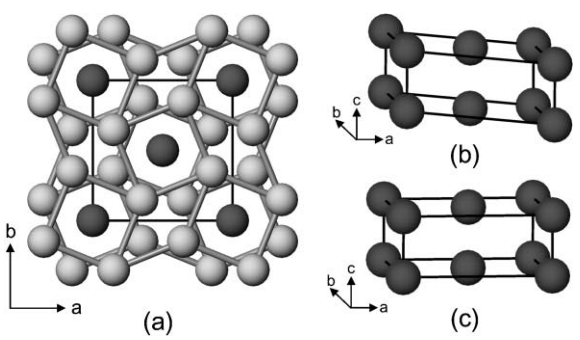

Fig. 2 (a) Structure of Ba-IVa shown in projection down the *c*-axis (see Ref. 30). The host atoms, in layers at $z = 0$ and ½, are shown using light grey shading and the guest atoms chains with dark grey shading. Insets: perspective views of the coexisting (b) monoclinic and (c) tetragonal guest structures in Ba-IVa.

incommensurate nature of the structure unequivocally.[34] A different structure of the same type was first discovered in Rb[32] and has since been found in K.[33] In these elements, the host structure has the same tetragonal *I*4/*mcm* space group as in Ba, Sr, Sc and Bi, but is made up of 16 atoms.[32,33] The Rb-IV structure at 16.8 GPa is shown in projection down the *c* axis in Fig. 3a with host atoms on the 16*k* site of *I*4/*mcm* at (0.7903(1),0.0851(1),½) in a unit cell with lattice parameters $a_H = b_H = 10.3503(1)$ Å and $c_H = 5.1865(2)$ Å.[32] The guest structure is body-centered tetragonal, space group *I*4/*mmm*, with $a_G = b_G = a_H$ and $c_G = 3.1797(6)$ Å (Fig. 3b).

Although the general arrangement of the host framework is the same in all eight elements, as illustrated in Figs. 2 and 3, various different guest structure arrangements are made possible by the freedom of the guest chains to adopt different relative positions along the *c*-axis. As seen in Ba-IVa, there can even be a clearly monoclinic guest, with a β angle of $\sim 96^\circ$, in a host that is not detectably distorted from tetragonal symmetry.

A more complete and rigorous description of these structures can be obtained within the formalism of 4-D superspace, in which the periodicity of incommensurate structures of this kind is recovered in a 4-dimensional space.[38] Diffraction peaks are then indexed using four Miller indices (*hklm*), instead of three, and the symmetry is described using 4-D superspace groups. The reflections from the 'host' and 'guest' components of the structure are indexed as (*hkl*0) and (*hk*0*m*), respectively. The other, general (*hklm*) reflections arise from modulations attributable to interactions between the host and guest components. These reflections are often very weak, but are important to a full structural description and their intensity gives a direct indication of the strength of the host–guest interaction. A complete description can thus be obtained either in terms of a single structure in 4-D superspace, or in terms of separate 3-D host and guest components plus a mutually modulating interaction between them. The former is required for full structure refinement and formal description, but we will continue to use the latter where it aids discussion and comparison of structures. A detailed account of superspace methods is beyond the scope of this article, but can be found in the comprehensive review by van Smaalen.[38]

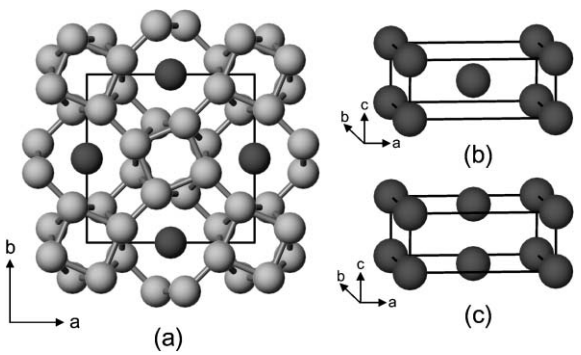

Fig. 3 (a) Structure of Rb-IV shown in projection down the *c*-axis (see Ref. 32). The host atoms, in layers at $z = 0$ and ½, are shown using light grey shading and the guest atoms chains with dark grey shading. Insets: perspective views of the (b) body-centred and (c) face-centred guest structures in Rb-IV and K-III, respectively.

The superspace groups of the coexisting phases of Ba-IVa with the *C*-face centred tetragonal and monoclinic guest structures are, respectively, *I*4/*mcm*(00q_3)0000, with $q_3 = c_H/c_G = 1.3884(2)$, and *I*2/*c*($q_1$0$q_3$)00, with $q_1 = (a_G\cos\beta_G - a_H\cos\beta_H)/c_G = 0.263(2)$[39] and $q_3 = 1.3823(3)$ at 12.1 GPa.[37] In the latter case, the description in a monoclinic superspace group underlines that both host and guest structures have to be treated as monoclinic, although we have observed no detectable evidence of any deviation of the host structure from tetragonal symmetry. Sr-V and Sc-II also have *C*-face centred tetragonal guest structures,[31,36] and they have superspace group *I*4/*mcm*(00q_3)0000 with $q_3 = 1.404(1)$ at 56 GPa and with $q_3 = 1.2804(3)$ at 23 GPa, respectively.[31,36] Bi-III has a body-centred tetragonal guest structure, which leads to a superspace group symmetry *I*′4/*mcm*(00q_3)0000, where *I*′ denotes the centring (½,½,½,½) in superspace and $q_3 = 1.309(1)$ at 6.8 GPa.[34,37] Sb-IV and As-III differ in having a host structure with a small but readily measurable distortion from tetragonal to monoclinic. The host and guest components are both body-centred monoclinic, with 3-D space groups *I*2/*c* and *I*2/*m* respectively, and the resulting superspace group is *I*′2/*c*($q_1$0q_3)00, with $q_1 = 0.1662(1)$ and $q_3 = 1.3132(1)$ in Sb-IV at 6.9 GPa, and with $q_1 = 0.1162(3)$ and $q_3 = 1.3047(1)$ in As-III at 50 GPa, respectively.[35,37,40]

The Rb-IV guest structure is body-centered tetragonal, space group *I*4/*mmm*, and the superspace group of the full structure is *I*′4/*mcm*(00q_3)000*s* with $q_3 = 1.631(2)$ at 16.8 GPa.[32,37] In K-III, the guest structure is also tetragonal, but *C*-face centred (Fig. 3c), with 3-D space group *C*4/*mmm*. The resulting superspace group is then *I*4/*mcm*(00q_3)000*s*, with $q_3 = 1.603(2)$ at 22.1 GPa.[33]

An aspect of composite structures is that, because the host and guest components are incommensurate along *c*, the host unit cell contains a non-integer number of atoms. The total is made up of 8 host atoms (or 16 in Rb and K) and $2 \times (c_H/c_G)$ guest atoms so that in Ba-IVa at 12.1 GPa, for example, the structure with the monoclinic guest component has 10.76 atoms per host unit cell. This has solved some longstanding puzzles about the density of some phases—in Bi-III and Sb-II, for instance.[34] Because the host component (with its greater number of atoms) gives much stronger diffraction peaks than does the guest component, earlier attempts to solve the structures of these phases yielded non-composite solutions based on an integer number of atoms in the host unit cell. These failed to give calculated densities in agreement with Bridgman's measurements, whereas the host–guest structures provide strikingly good agreement.[34] Another, and intriguing, feature of this type of structure is that any difference in pressure dependence between c_H and c_G causes the total number of atoms in the host unit cell to change. In Ba-IVa, c_H is more compressible than c_G, so that increasing pressure must cause guest atoms to be squeezed out of the structure; and decreasing pressure must somehow draw atoms into the host channels.

2.2 Incommensurate modulated structures

The only element known to have an incommensurate modulated structure at ambient pressure is uranium, in which

a phase of this kind occurs at low temperatures, below 43 K.[41] Under pressure, this type of structure has been found so far in the group 16 elements Te,[20] Se[42] and S.[43] (It has also been observed in iodine[44] and bromine[45] under pressure, but neither of these structures is described here.) A structure of this type can be regarded as a basic 3-D structure with the atoms displaced by a modulation wave, the wavelength of which is incommensurate with the basic structure repeat. As a consequence, the atomic positions in every unit cell of the structure are slightly different, and the diffraction pattern contains reflections from the average structure, and other 'satellite' reflections arising from the modulation. This is to be distinguished from the incommensurate composite structures where the incommensuration arises from the different periodicities of the component structures and the modulations are relatively weak. In that case, the (*hklm*) modulation reflections are very weak, and often too weak to measure, whereas in the incommensurate modulated case the satellite reflections can often be comparable in intensity with many of those from the average structure—which can make solution from powder diffraction data almost impossible. These structures thus generally require single-crystal data in order to determine the structures, whereas the weakness of the modulation reflections in the composite structures enables the structures to be solved from powder data once the possibility of the structure type is known.

In uranium, the modulated phase is believed to arise as a result of a charge density wave (CDW).[41] The average structure of the incommensurate phase is orthorhombic, space group *Cmcm*, with atoms on the $\pm(0,y,¼)$ positions, with $y \sim 0.1023(2)$ at room temperature.[2] This average structure is shown in Fig. 4. The modulation of the structure is extremely complex, and has been the subject of a number of detailed neutron diffraction studies,[2,46,47] and the q-vector of the CDW is given by $\boldsymbol{q} = q_x\boldsymbol{a}^* \pm q_y\boldsymbol{b}^* \pm q_z\boldsymbol{c}^*$, where $q_x = 0.500(1)$, $q_y = 0.176(2)$ and $q_z = 0.182(2)$ at 5 K.[41] More recently, is has been shown that $q_x = 0.495(3)$ at 40 K,[47] and that, while q_y and q_z are temperature dependent above 22 K, they lock into commensurate values of 1/6 (0.1666) and 5/27 (0.1852), respectively, below that temperature.[47]

The modulated phases of Te, Se and S all have the same incommensurate structure, different from that in U, as first observed in Te-III.[37,20] We made many unsuccessful attempts to solve this structure from powder data, and the true

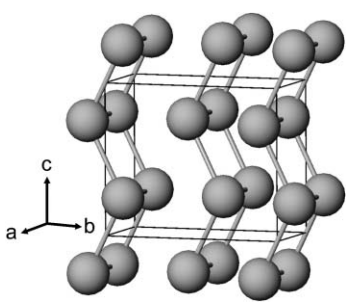

Fig. 4 Average crystal structure of α-uranium (see Ref. 41). Contact distances up to 2.9 Å are shown as solid lines. The incommensurate modulation of the structure is not shown.

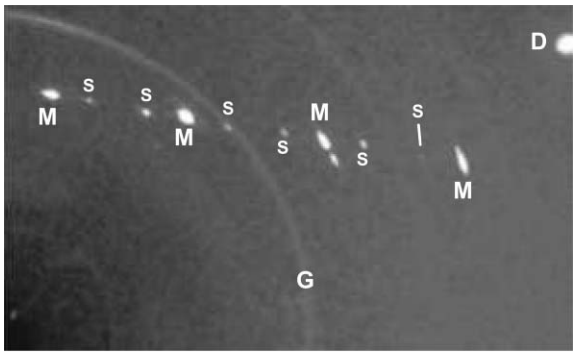

Fig. 5 Part of the diffraction pattern from a quasi-single crystal of Te-III at 7.4 GPa showing the main (M) and satellite (S) Bragg reflections. The peak marked with a "D" is from one of the diamond anvils in the pressure cell, and the diffraction ring marked "G" is from the metal gasket.

incommensurate nature of the structure was recognised only after a quasi-single crystal of Te-III was obtained at 7.4 GPa, and data from it revealed clear evidence of satellite reflections at $(h,k\pm q_2,l)$, with $q_2 \sim 0.3$ at 7.4 GPa (Fig. 5).[20] The basic 3-D structure is body-centred monoclinic, space group *I*2/*m*, with atoms on the 2*a* sites at (0,0,0). Refinement of powder-diffraction data then showed the superspace group of the Te-III structure to be $I'2/m(0q_20)s0$, with $a = 3.9181(1)$ Å, $b = 4.7333(1)$ Å, $c = 3.0612(1)$ Å, $\beta = 113.542(2)^\circ$ and $q_2 = 0.2880(2)$ at 8.5 GPa, where $(0q_20)$ is the wavevector of the incommensurate modulation.[20] Only first-order modulation reflections are observed, and the modulation can therefore be described using two first-order Fourier components $B_{1x} = 0.0215(9)$ and $B_{1z} = 0.0925(7)$.[20] The resulting structure is illustrated in Fig. 6 which shows four unit cells of the basic structure, and the effects of the modulation wave. (Fig. 19 below provides another view of the same structure in which the variation in position along the *c*-axis through the modulation wave is shown in terms of the refined *z* coordinates.) This structure has also been observed in Se-IV above 28 GPa[42] where $a = 3.2511(1)$ Å, $b = 4.0026(1)$ Å, $c = 2.5735(1)$ Å, $\beta = 113.277(3)^\circ$, $q_2 = 0.2886(5)$, $B_{1x} = 0.0236(11)$ and

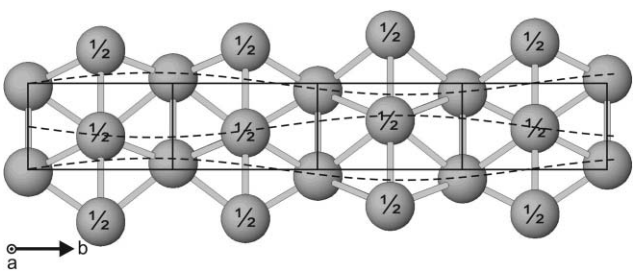

Fig. 6 Four unit cells of the modulated structure of Te-III at 8.5 GPa, as shown in projection down the monoclinic *a*-axis (see Ref. 20). Atoms in the body-centre position are labelled with "½". The modulation wave, (0,0.2880(2),0), is indicated with the dashed lines. *Note: The displacements of the atoms labelled "½" were shown incorrectly in Refs. 20, 37, 42 and 85, though the description in terms of structural parameters was correct. These atoms are displaced in anti-phase to those at the corners of the unit cell, and not in phase as previously shown.*

B_{1z} = 0.0900(8) at 42 GPa, and in S-III above 75 GPa,[43] where a = 2.802(1) Å, b = 3.455(1) Å, c = 2.208(1) Å, β = 113.15(1)°, q_2 = 0.281(1) B_{1x} = 0.028(1) and B_{1z} = 0.118(1) at 100.5 GPa.[43]

2.3 Modulated layer structures

Structures made up of various different stacking sequences of similar 8-atom and 10-atom layers have been found at high pressure in Cs,[18] Rb[19] and Ga.[49] No structures of this kind are known in elements at ambient pressure. There is also a high-pressure structure in Li[50] that can be regarded as a stacking of just the 8-atom layers, and thus as an unmodulated end member of the group.[49]

The first member of this group was found as the structure of Cs-III.[18] It is *C*-face-centred orthorhombic, space group $C222_1$, with 84 atoms in the unit cell. At 4.3 GPa the refined lattice parameters are a = 9.2718(1) Å, b = 13.3013(3) Å, and c = 34.2025(7) Å, with four atoms located on a fourfold 4*b* site, and the remaining eighty occupying ten eightfold 8*c* sites. The atomic coordinates are given in Ref. 18. The structure, shown in Fig. 7a, comprises 10 layers of atoms stacked along the *c*-axis—two symmetry related 10-atom layers (shown in black), and two different sets of four symmetry-related 8-atom layers (identified using different shades of grey). The complexity of this structure is such that it could only have been determined using single-crystal techniques, and we utilised the low melting temperature of Cs at ~4 GPa to grow a single-crystal sample.

The second member of this family was found in Rb-III.[19] Like Ba-IV, this phase gives strongly textured diffraction patterns, and we exploited this to grow a quasi-single crystal of the phase at 14.3 GPa. The space group is $C222_1$, the same as Cs-III, with refined lattice parameters of a = 7.886(2) Å, b = 11.240(2) Å, and c = 18.431(2) Å at 14.3 GPa. There are 52 atoms in the unit cell, with four located on a 4-fold 4*b* site and the remaining 48 being located on six different eightfold 8*c* sites. The atomic coordinates are given in Ref. 19, and the refined structure is shown in Fig. 7b. It can be seen to be remarkably similar to that of Cs-III except that the two 10-atom layers are stacked with only one set of four 8-atom layers. It is readily apparent that the arrangement of atoms in layers 1, 2, 3, and 4 of Rb-III is closely similar to that in layers 2, 3, 4, and 5 of Cs-III. As in the case of Cs-III, it is unlikely that this structure could have been determined other than with single-crystal techniques.

The most complex member of this group of structures was found in Ga-II,[49] a structure long reported to be body-centred cubic,[51] but shown—again using single-crystal techniques—to have a *C*-face-centred orthorhombic structure, space group $C222_1$ as for Rb-III and Cs-III, with 104 atoms per unit cell.[49] The refined lattice parameters at 2.8 GPa are a = 5.976(1) Å,

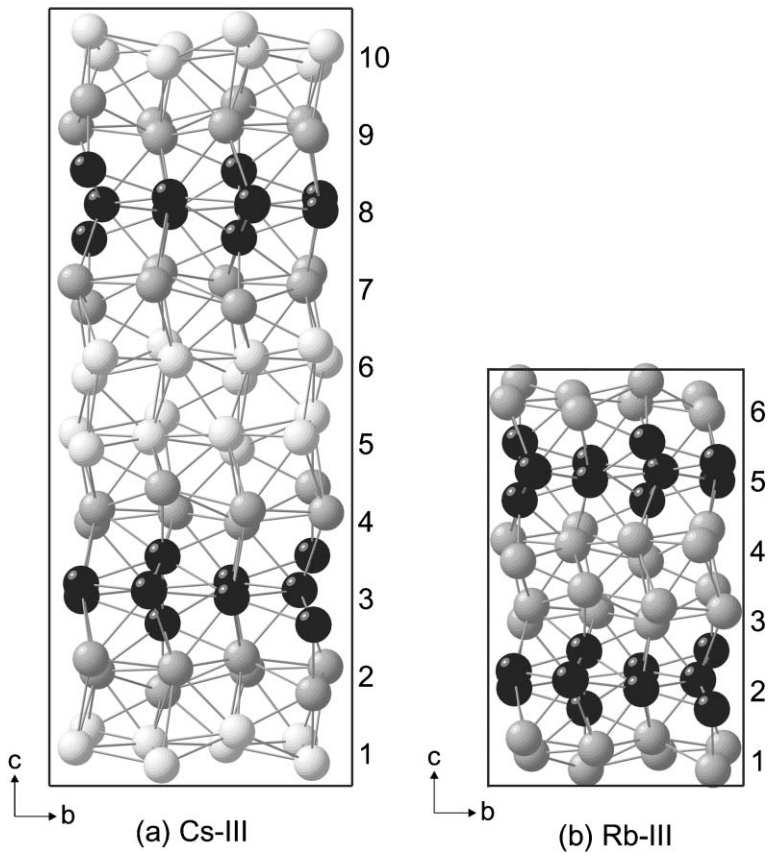

Fig. 7 (a) Crystal structure of Cs-III as viewed along the *a*-axis of the orthorhombic unit cell (see Ref. 18). Contact distances up to 4.7 Å are shown as solid lines. The 8- and 10-atom layers are numbered and non-equivalent 8-atom layers are in two different shades of light grey. (b) Crystal structure of Rb-III as viewed along the *a*-axis of the orthorhombic unit cell (see Ref. 19). Contact distances up to 4.1 Å are shown as solid lines. The 8- and 10-atom *a*–*b* layers are numbered. Further details of the structures, including atomic coordinates and the structure of the individual *a*–*b* layers can be found in Ref. 18 and 19.

b = 8.576(1) Å and c = 35.758(3) Å, with eight atoms located on two different 4-fold 4*b* sites and the 96 others occupying twelve eightfold 8*c* sites. The atomic coordinates are given in Ref. 49, and the structure is shown in Fig. 8. It can be understood in terms of stacking of 8- and 10-atom layers that are very similar to those in Rb-III and Cs-III, but with an additional set of 10-atom layers (such as 1 and 7 in Fig. 8).

The final member of this family of structures is the body-centred cubic structure observed in lithium above 42 GPa.[50] This structure has space group $I\bar{4}3d$ with 16 atoms occupying the 16*c* sites at (x,x,x) with x = 0.055. The lattice parameter at 38.9 GPa is a = 5.2716 Å.[50] This structure is shown in Fig. 9,

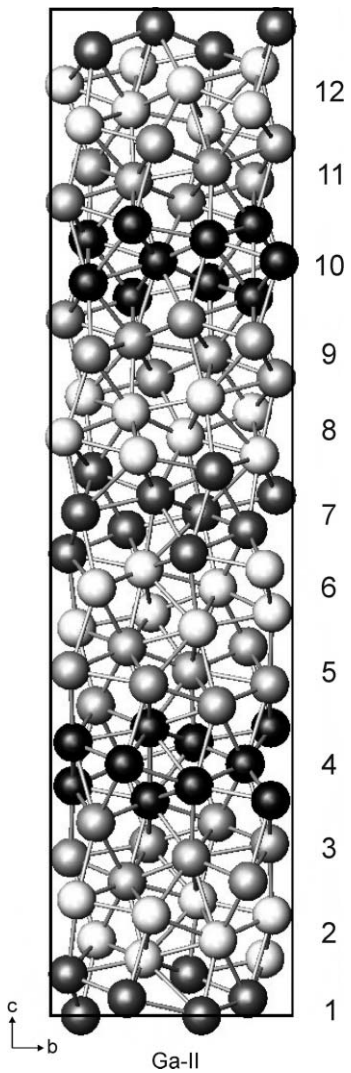

Fig. 8 Crystal structure of Ga-II as viewed along the *a*-axis of the orthorhombic unit cell (see Ref. 49). Contact distances up to 3.3 Å are shown as solid lines. The 8- and 10-atom *a*–*b* layers are numbered. Non-equivalent 8-atom layers are in two different shades of light grey. The 10-atom layers in black are oriented like those in Cs-III and Rb-III (see Fig. 7); the 10-atom layers in dark grey—unique to Ga-II—have essentially the same arrangement of atoms, but are rotated 90° around the *c* axis, compressed a little along *a* and stretched a little along *b*. Further details of the structure, including atomic coordinates and the structure of the individual *a*–*b* layers, can be found in Ref. 49 of Section 2.3.

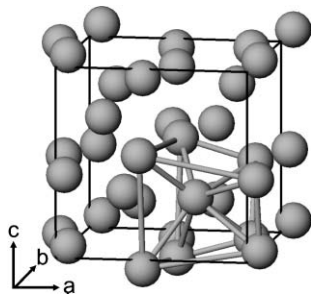

Fig. 9 Crystal structure of Li-IV (see Ref. 50). The structure can be regarded as a distorted 2 × 2 × 2 superstructure of the *bcc* structure, and one of the eight distorted-*bcc* sub-units is highlighted with grey solid lines.

and is a simple distortion of a 2 × 2 × 2 superstructure of the body-centered cubic (*bcc*) structure, with each atom shifted 0.05 in fractional coordinates along one of the *bcc* [111] directions.

2.4 Other complex and non-simple-close-packed structures

2.4.1 Cs-IV. The Cs-IV structure is observed in both Cs[52] and Rb[53] at high pressure. It is body-centred tetragonal, space group $I4_1/amd$, with four atoms per unit cell located on the 4*a* site at (0,0,0).[52] The lattice parameters in Cs-IV at 8.0 GPa are a = 3.349(6) Å and c = 12.487(30) Å,[52] while in Rb at 28 GPa they are a = 2.883 Å and c = 10.760 Å.[53] The space group and atomic positions are the same as the β-tin structure (see section 2.4.3), but the Cs-IV structure is greatly elongated along the *c*-axis. The structure is shown in Fig. 10.

2.4.2 Cs-V. The Cs-V structure is observed in Cs,[54] Rb,[55] and also in Si[56] and Ge[57] at high pressures. It is *C*-face centred orthorhombic, space group *Cmca*, with atoms located on the 8*f* (0,y,z) and 8*d* (x,0,0) sites.[56] In Cs-V at 19.6 GPa, the refined lattice parameters are a = 10.879(3) Å, b = 6.443(2) Å and c = 6.389(2) Å with the atoms located at (0,0.1781(2),0.328(2)) and (0.2118(2),0,0).[54] In Rb-VI at 48.1 GPa, a = 9.3718(10) Å, b = 5.5501(6) Å and c = 5.5278(6) Å with the atoms located at

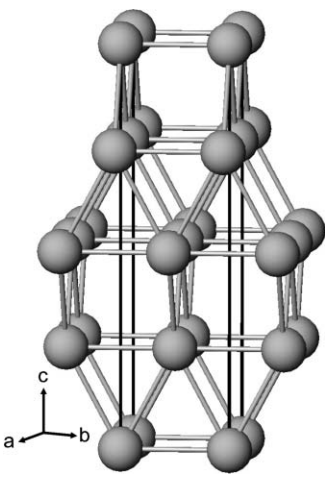

Fig. 10 Crystal structure of Cs-IV (see Ref. 52). Contact distances up to 3.6 Å are shown as solid lines.

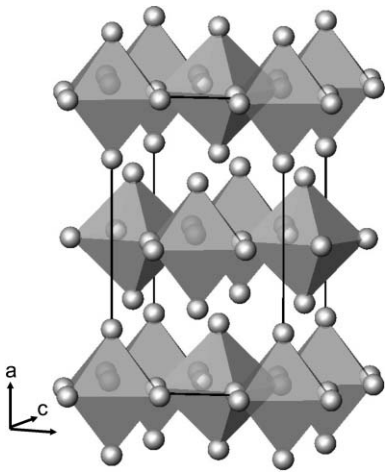

Fig. 11 Crystal structure of Cs-V (see Ref. 54). The corner-sharing octahedra are shown shaded.

(0,0.1704(9),0.3177(9)) and (0.2107(4),0,0).[55] The structure is shown in Fig. 11, and can be regarded as a distortion of a $\sqrt{2} \times \sqrt{2}$ superstructure of *fcc*, and comprises layers of corner-sharing octahedral groups lying in the orthorhombic *b*–*c* plane and stacked along the *a*-axis.[54]

2.4.3 β-Tin. Sr above 24 GPa[58] adopts the β-tin structure that is found in tin above 291 K at ambient pressure.[2] This structure is also observed in Si and Ge at high pressures.[59] The structure is body-centred tetragonal, space group $I4_1/amd$, with atoms on the 4*a* site at (0,0,0). In Sn at 298 K at ambient pressure, a = 5.8316(2) Å and c = 3.1815(2) Å.[2] In Sr-III at 34.8 GPa, a = 5.504(2) Å and c = 2.960(2) Å.[58] The β-tin structure is described in detail by Donohue.[2]

2.4.4 Sr-IV. The Sr-IV structure is unique to Sr where it is observed above 35 GPa.[60] It is body-centred monoclinic, space group *Ia*, with 12 atoms located on three 4*a* (*x*,*y*,z) sites. The structure can be viewed as a helical distortion of the tetragonal β-tin structure (Sr-III), in which atoms lying in (straight) chains along the Sr-III *c*-axis displace to form helical chains.[60] At 41.7 GPa, the lattice parameters are a = 5.7456(2) Å, b = 7.8009(2) Å, c = 5.5370(3) Å, β = 96.990(2)° and the coordinates of the three independent atoms are (0.3039(13), 0.1574(11), 0.6322(21)), (0.4787(17), 0.5784(7), 0.4645(36)) and (0.6840(8), 0.1445(11), 0.3459(19)). An excellent fit can be obtained using a constrained model, with only a single variable atomic coordinate, in which all atoms displace equal distances from their β-tin positions in directions 120° apart in the $(\bar{1}01)$ plane—with one of the displacements along the Sr-III *a*-axis direction (a_{III} in Fig. 12). This model is fully described in Ref. 60. Using this constrained model, the refined atomic coordinates at 41.7 GPa are (0.3031(2), 0.1545(3), 0.6353(3)), (0.4889(1), 0.5847(4), 0.4885(1)) and (0.7079(4), 0.1358(1), 0.3762(4)).[60] The structure is shown in Fig. 12.

2.4.5 Sc-V. The Sc-V structure is unique to Sc, where it is observed above 240 GPa.[61] It is hexagonal, space group $P6_122$ or $P6_522$, with atoms located on the 6*a* site at (*x*,0,0).[61] At 242 GPa, the lattice parameters are a = 2.355(1) Å and

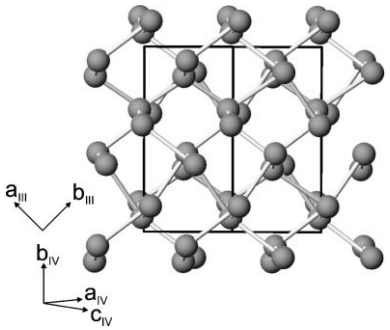

Fig. 12 Crystal structure of Sr-IV as viewed along the *c*-axis direction of the Sr-III structure, revealing the helical distortion along this direction (see Ref. 60). The atoms in the helical chains are equally spaced along the direction of view. Contact distances up to 3 Å are shown as solid lines.

c = 10.446(3) Å, and x = 0.461(1).[61] The structure comprises chains along the *c*-axis, in which each atom has two nearest neighbours within the chain, and two slightly further away in neighbouring chains, and can be regarded as a distortion of the *fcc* structure.[61] The structure is shown in Fig. 13.

2.4.6 ω-Ti. The ω-Ti structure is observed in all of the group 4 elements (Ti, Zr and Hf) at high pressure, where it is observed above 7–9 GPa in Ti, 6.7 GPa in Zr, and 46–58 GPa in Hf.[62–66] It is hexagonal, space group *P6/mmm*, with three atoms per unit cell located on the 1*a* site at (0,0,0) and the 2*d*

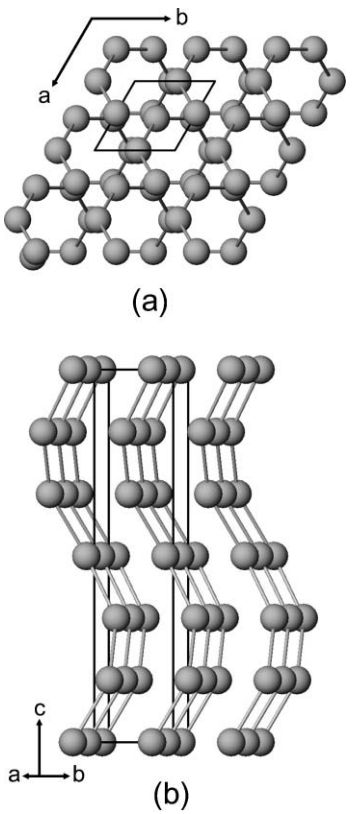

Fig. 13 Crystal structure of Sc-V as viewed (a) along, and (b) perpendicular to, the *c*-axis (see Ref. 61). Contact distances up to 2.1 Å are shown as solid lines.

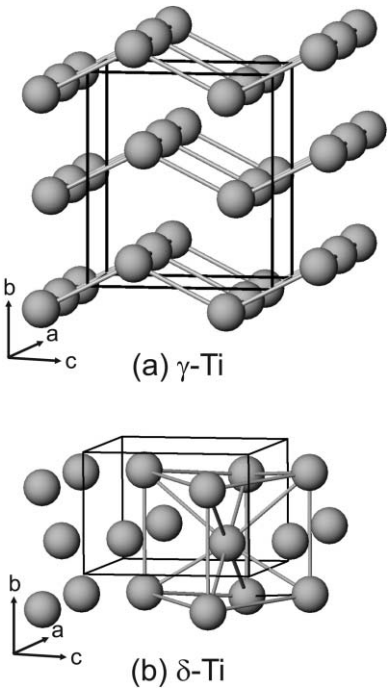

Fig. 14 Crystal structures of (a) γ-Ti (see Ref. 65) and (b) δ-Ti (see Ref. 66). For γ-Ti contact distances up to 2.4 Å are shown as solid lines. For δ-Ti the related *bcc* unit cell is shown with solid grey lines.

site at (½,⅔,½). No lattice parameters are reported for the ω-phases in any of these metals at high pressure. At atmospheric pressure, where the ω-phases are metastable in Ti and Zr, a = 4.625 Å and c = 2.813 Å, and a = 5.036 Å and c = 3.109 Å, respectively.[62] The structure is described in detail in Donohue.[2]

2.4.7 γ-Ti. The γ-Ti structure is observed only in Ti at pressures above 116(4) GPa.[65] The structure, which can be regarded as a distortion of the *hcp* structure, is *C*-face-centred orthorhombic, space group *Cmcm*, with atoms located on the 4*c* sites at (0,y,¼). In γ-Ti at 130 GPa, a = 2.382(1) Å, b = 4.461(5) Å, c = 3.876(4) Å and y = 0.11(1).[65,66] The structure comprises zigzag layers of atoms, and is shown in Fig. 14a.

2.4.8 δ-Ti. The δ-Ti structure is observed only in Ti above 140 GPa.[66] Like γ-Ti, it is *C*-face centred orthorhombic, space group *Cmcm*, with atoms located on the 4*c* sites at (0,y,¼). However, the lattice parameters and atomic coordinate are very different. In δ-Ti at 178 GPa, a = 3.8610(7) Å, b = 2.6296(6) Å, c = 3.6323(4) Å and y = 0.295(9)[66] and the structure can be regarded as an orthorhombic distortion of the *bcc* structure, and becomes identical to it if $a/b = c/b = \sqrt{2}$ and y = 0.25.[66] The δ-Ti structure, and its relationship to the *bcc* structure, is shown in Fig. 14b.

2.4.9 α-Mn. At ambient pressure, manganese has a crystal structure observed in no other element, under either ambient or high-pressure conditions. The α-Mn structure is cubic, space group $I\bar{4}3m$, with 58 atoms per unit cell.[2] The lattice parameter at ambient conditions is a = 8.9129(6) Å, and atoms are located on a number of different crystallographic sites: two on a 2*a* site at (0,0,0), 8 on an 8*c* site at (x_1,x_1,x_1); and the remaining 48 on two 24*g* sites at (x_2,x_2,z_2) and (x_3,x_3,z_3).[2] The refined atomic coordinates are x_1 = 0.31765(12), x_2 = 0.35711(8), z_2 = 0.03470(11), x_3 = 0.08968(8) and z_3 = 0.28211(11).[67] The details of the structure are complex, and are described fully in Donohue.[2]

2.4.10 α-Hg. Mercury is a liquid at ambient conditions but crystallises into the α-Hg structure on compression to 1.2 GPa at room temperature.[68] The same phase is observed at ambient pressure on cooling below 234 K. Hg-I is rhombohedral, space group $R\bar{3}m$ (hexagonal setting), with 6 atoms located on the 6*b* sites at (0,0,0).[69] The structure can be regarded as a distortion of the *fcc* structure, in which compression along the body-diagonal increases the rhombohedral angle from 60°. In Hg at ambient pressure and 78 K, a = 3.4645 Å, c = 6.6772 Å, and the rhombohedral angle is 70.7°.[69] There are no reported lattice parameters for α-Hg at high pressure. But the same structure is observed in Li-III above 39 GPa,[50] where the hexagonal lattice parameters at 39.8 GPa are a = 2.4023 Å and c = 5.51592 Å[50] and the rhombohedral angle is 62.87°. This structure is described in detail in Donohue.[2]

2.4.11 β-Hg. The β-Hg structure is observed in mercury above 3.4 GPa at room temperature and below 79 K at ambient pressure.[68] It is body-centred tetragonal, space group *I*4/*mmm*, with a = 3.995(4) Å and c = 2.825(3) Å at atmospheric pressure and 77K, and the atoms are located on the 2*a* sites at (0,0,0).[70] There are no reported lattice parameters for β-Hg at high pressure. This structure is the same as that of In-I and Ga-III (see 2.4.15), but with a compressed *c*-axis. This structure is described in detail in Donohue.[2]

2.4.12 γ-Hg. γ-Hg is observed only in mercury above ~12 GPa.[71] It is orthorhombic, with a = 2.691 Å, b = 4.457 Å and c = 6.454 Å at 19.8 GPa.[71] There is currently no space group information available and the structure is unsolved.

2.4.13 Ga-I. The Ga-I structure is unique to the ambient-pressure phase of Ga. It is orthorhombic, space group *Cmca*, with atoms located on the 8*f* (0,y,z) site at (0,0.1539(13), 0.0798(11)), and lattice parameters a = 4.5192 Å, b = 7.6586 Å, and c = 4.5258 Å.[2] The structure can be presented as a stacking of distorted close-packed layers in which each atom has a single close neighbour, and has thus also been described in terms of singly bonded Ga_2 units. The details of the structure are described fully in Donohue.[2]

2.4.14 Ga-V. Ga-V occurs at pressures above 10.5 GPa[49] and has a rhombohedral structure, space group $R\bar{3}c$ (hexagonal setting), with atoms located on the 18*e* site at (x,0,¼). At 12.2 GPa, x = 0.187(2) and the lattice parameters are a = 8.3272(3) Å and c = 4.7222(2) Å.[49] The rhombohedral angle at 12.2 GPa is 110.78°, and the structure is only slightly distorted from body-centred cubic, where the rhombohedral angle would be 109.47°. The structure is shown in Fig. 15.

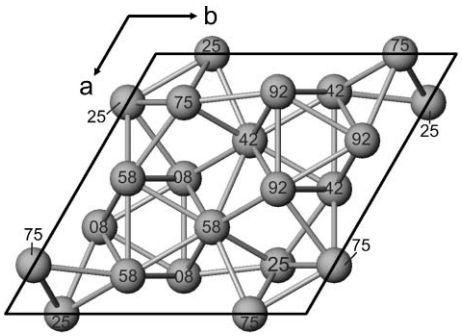

Fig. 15 Crystal structure of Ga-V as viewed along the *c*-axis (see Ref. 49). The numbers on each atom give the *z* coordinates in units of 0.01. Contact distances up to 3 Å are shown as solid lines.

2.4.15 In-I. Ga-III above 2 GPa adopts the In-I structure found in In at ambient conditions. This is body-centred tetragonal (bct), space group *I*4/*mmm*, with atoms located on the 2*a* sites at (0,0,0).[2] In In-I at ambient pressure, the lattice parameters are a = 3.2520(6) Å and c = 4.9470(11) Å, with c/a = 1.5212(3).[2] In Ga-III at 2.8 GPa, the lattice parameters are a = 2.808(3) Å and c = 4.458(3) Å with c/a = 1.588.[72] The In-I structure is only slightly distorted from the *fcc* structure, and the two would be equivalent for $c/a = \sqrt{2} = 1.414$. The relationship between the two structures is shown in Fig. 16. See also the β-Hg structure in 2.4.11. A structure with the same space group and atomic coordinates is observed in tin above 9.2 GPa where a = 3.70(1) Å and c = 3.37(1) Å in Sn-III at 9.8 GPa.[73] The c/a ratio 0.911(4) is close to unity, and thus the Sn-III structure can be regarded as a tetragonal distortion of *bcc*.

2.4.16 In-II. The In-II structure is observed only in indium above 45 GPa.[74a] It is orthorhombic, space group *Fmmm*, with 4 atoms located in the 4*a* sites at (0,0,0).[74a] The lattice parameters at 93(5) GPa are a = 3.769(3) Å, b = 3.846(3) Å and c = 4.140(4) Å.[74a] In-II can be regarded as an orthorhombic distortion of a $\sqrt{2}a \times \sqrt{2}a \times c$ supercell of the tetragonal In-I structure, and thus as an orthorhombic distortion of the *fcc* structure. The relationship between In-I and In-II is then as shown in Fig. 16.

2.3.17 As-I. The structure of As, Sb and Bi at ambient conditions is trigonal, space group $R\bar{3}m$ (hexagonal setting),

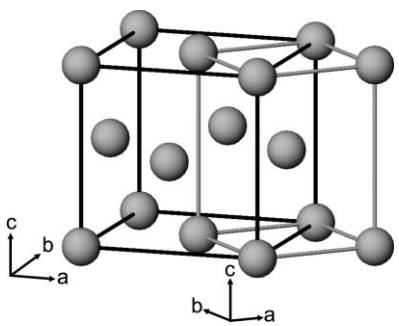

Fig. 16 Crystal structure of In-I. The body-centred tetragonal unit cell is outlined in grey, while the alternative face-centred tetragonal cell is outlined in black. The In-II structure (see Ref. 74a) is an orthorhombic distortion of this face-centred cell.

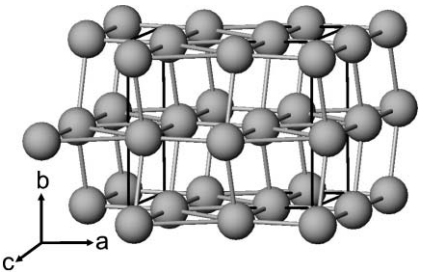

Fig. 17 Crystal structure of Bi-II (see Ref. 75). Contact distances up to 3.8 Å are shown as solid lines.

with atoms located on the 6*c* sites at (0,0,*z*).[2] In As-I, a = 3.7599(1) Å, c = 10.5478(10) Å and z = 0.2271, while, in Sb-I, a = 4.3081(8) Å, c = 11.2737(6) Å and z = 0.2335, and in Bi-I a = 4.5461(2) Å, c = 11.8623(4) Å and z = 0.2339.[2] The same structure is also found in P above 5.5 GPa,[74b,74c] where a = 3.398(4) Å, c = 8.748(12) Å and z = 0.223(3) at 6.7 GPa.[74c] The structure can be regarded as a small distortion of the primitive cubic α-Po structure (see 2.4.23), the two structures becoming identical if $c/a = \sqrt{6} = 2.449$ and z = ¼. The structure is described in detail by Donohue.[2]

2.4.18 Bi-II. The Bi-II structure is observed only in Bi at high pressure. The structure is *C*-face-centred monoclinic, space group *C*2/*m*, with atoms located on the 4*i* sites at (*x*,0,*z*).[75] The refined structural parameters at 2.7 GPa are a = 6.6584(2) Å, b = 6.0982(2) Å, c = 3.2965(1) Å, β = 110.37(2)°, x = 0.2489(3) and z = 0.1372(5).[40] The structure is shown in Fig. 17.

2.4.19 Sulfur. The equilibrium structure of sulfur at ambient conditions is face-centred orthorhombic, space group *Fddd*, with a = 10.4646(1) Å, b = 12.8660(1) Å and c = 24.4860(3) Å.[76] The atoms are located on 4 different 32*h* positions at (*x*,*y*,*z*), and the unit cell contains 128 atoms arranged in puckered S_8 ring-shaped molecules. The atomic coordinates are given in Ref. 76, and the complex structure is described in detail by Donohue.[2]

2.4.20 S-II. The S-II structure is observed as an equilibrium structure in sulfur above 35–38 GPa.[77,175] It is tetragonal, space group $I4_1/acd$, with atoms located on the 16*f* site at (*x*,*x*,¼). The refined structural parameters in S-II at 55 GPa are a = 7.841(1) Å, c = 3.100(1) Å and x = 0.136(1).[77] The structure is shown in Fig. 18 and comprises 'square' chains around 4_1 and 4_3 screw symmetry axes running along the *c*-axis.

2.4.21 Se-I. The structure of both Se and Te at ambient conditions is trigonal, space group $P3_121$ (hexagonal setting), with atoms located on the 3*a* sites at (x,0,⅓).[2] In Se-I, a = 4.3655(10) Å, c = 4.9576(24) Å and x = 0.2254(10); in Te-I, a = 4.4561(12) Å, c = 5.9271(13) Å and x = 0.2633(5).[2] The structure comprises helices running along the *c*-axis and can be regarded as a distortion of the primitive cubic structure. The two structures would be identical if $c/a = \sqrt{3/2} = 1.225$ and x = ⅓.[2] The structure is described in detail by Donohue.[2]

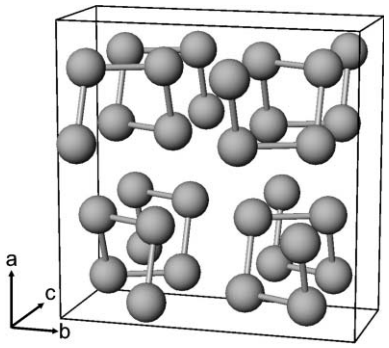

Fig. 18 Crystal structure of S-II at 55 GPa, showing 'square' chains around 4_1 and 4_3 screw symmetry axes running along the *c* axis (see Ref. 77). Contact distances up to 2 Å are shown as solid lines.

2.4.22 Te-II. Te,[78] Se[78] and S[43] at high pressures have a triclinic structure, one of only two triclinic structures reported in the elements at high pressures. It was solved through the use of high-pressure single-crystal methods, with data taken from the same sample as was used to determine the structure of Te-III (see 2.2 above). The only other known triclinic structure in the elements is that of Cf.[79] The Te-II structure has now been found at high pressure for Se-III and is probably also the structure of S-V.[43] To aid comparison with the Te-III structure, Te-II is described in a non-standard body-centred space group setting, $I\bar{1}$. At 4.5 GPa, the lattice parameters for Te-II are a = 4.0793(1) Å, b = 14.1981(3) Å, c = 3.0977(1) Å, α = 87.516(2)°, β = 112.536(2)° and γ = 91.098(2)°.[78] There are six atoms in the non-standard unit cell, located on the 2*a* (0,0,0) and 4*i* (*x*,*y*,*z*) sites with x = 0.5310(5), y = 0.1684(1) and z = 0.6198(5).[78] For Se-III at 25.6 GPa, the lattice parameters are a = 3.4648(1) Å, b = 12.0875(5) Å, c = 2.6481(1) Å, α = 86.805(5)°, β = 112.021(5)° and γ = 91.344(8)°, and the atoms are at (0,0,0) and (0.5393(7), 0.1685(2), 0.6372(7)).[78] In S-V at 63.7 GPa, the atomic coordinates have not yet been determined, but the lattice parameters are a = 2.966(8) Å, b = 10.666(3) Å, c = 2.284(2) Å, α = 86.67(2)°, β = 111.89(1)° and γ = 91.30(1)°.[43]

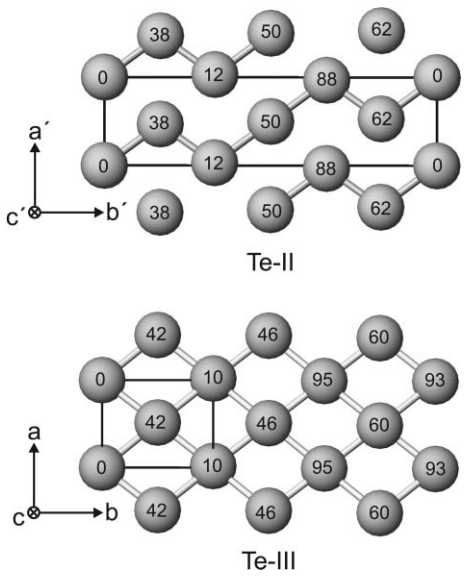

Fig. 19 Crystal structure of Te-II as viewed along the triclinic *c*-axis (see 2.4.22), with the *b*-axis inverted from the standard description to facilitate comparison with Te-III, as explained in the text. Three unit cells of the modulated structure of Te-III at 8.5 GPa, are shown for comparison. The numbers on each atom give the *z* coordinates in units of 0.01. Contact distances up to 3.3 Å are shown in both structures as solid lines. See also Fig. 6. *Note: The atomic coordinates shown for the Te-III structure differ from previous incorrect drawings in Refs. 20, 37, 42 and 85, and correspond to the corrected drawing in Fig. 6.*

The Te-II structure as viewed along the *c*-axis is shown in Fig. 19. To facilitate comparison with incommensurate Te-III, three units of which are shown, the Te-II structure has been drawn with the *b*-axis inverted from the standard description given above. The two structures are clearly closely related. The III→II transition involves a tripling of the Te-III unit cell along *b*, equivalent to the wave vector locking in at the commensurate value of q_2 = ⅓, with a slight distortion of both the α and γ cell angles of Te-III away from 90°, and small displacements of the atoms in the *a*–*c* plane.

2.4.23 α-Po. The structure of α-Po is primitive cubic, space group $Pm\bar{3}m$, with a = 3.352 Å at 283 K[2] and an atom located on the 1*a* site at (0,0,0). The atoms thus lie at the lattice points of a primitive cubic lattice. This structure is also observed in P above 10.0(6) GPa,[74b,74c] in Ca above 32 GPa[80] and in As above 25 GPa.[81] The lattice parameters of these three phases are a = 2.39(1) Å in P at 10.3 GPa,[74c] a = 2.615(2) Å in Ca at 39 GPa[80] and 2.465(4) Å in As at 36.6 GPa.[81] The structure is described in detail by Donohue.[2]

2.4.24 β-Po. S (Ref. 82) and Se (Ref. 83) at high pressures at room temperature, and Te at high pressures and temperatures above 315 K,[84] adopt the β-Po structure found in Po above 327 K.[2] This structure is rhombohedral, with space group $R\bar{3}m$ (hexagonal setting), and atoms located on the 3*a* site at (0,0,0).[2] In Po at atmospheric pressure and 348 K, a = 5.089(3) Å and c = 4.927(3) Å, with c/a = 0.968.[2] This structure can be regarded as distorted from primitive cubic, and the two would be identical for c/a = 1.225. In Se-IV at 87.9 GPa, the lattice parameters are a = 3.8920(3) Å and c = 2.9572(2) Å, with c/a = 0.760.[83] In Te-IV at 23.0 GPa and 473 K, a = 4.6873(3) Å and c = 3.5474(2) Å, with c/a = 0.757.[84] And in S-V at 160 GPa, a = 3.3780(1) Å and c = 2.6919(3) Å, with c/a = 0.797.[85] The c/a ratios of S-V, Se-IV and Te-IV are much further from the primitive cubic structure than in β-Po itself, and can instead be regarded as a *bcc* structure elongated along the body-diagonal: the structure would be the same as *bcc* for c/a = 0.61. This form of the β-Po structure, and its relationship to the *bcc* structure, are shown in Fig. 20.

3. Individual systems

3.1 Group I (Li, Na, K, Rb, Cs)

The alkali elements behave as nearly-free-electron metals at ambient pressure, where they all adopt the body-centred cubic (*bcc*) structure with lattice parameters a = 3.5091(4) Å (Li-I), a = 4.2906(5) Å (Na-I), a = 5.321 Å (K-I), a = 5.703(7) Å (Rb-I) and a = 6.141(7) Å (Cs-I) at room temperature.[89] On compression, the first transition in each case is to the

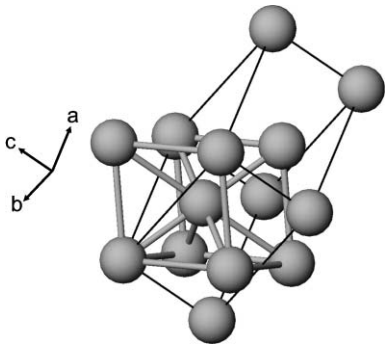

Fig. 20 Crystal structure of β-Po. The distorted *bcc* structure is highlighted with solid lines.

fcc structure at 6.9 GPa (Li-II),[86] 65 GPa (Na-II),[87] 11 GPa (K-II),[53] 7 GPa (Rb-II)[53] and 2.37 GPa (Cs-II).[88] The lattice parameters of the *fcc* phases are a = 3.900(3) Å in Li-II at 8.0 GPa,[86] a = 3.5348(3) Å in Na-II at 85.6 GPa,[87] a = 5.130(2) Å in K-II at 11.7 GPa,[53] a = 5.224(2) Å in Rb-II at 11.9 GPa and a = 5.984(11) Å in Cs-II at 4.1 GPa.[88]

Diffraction studies of Li above 20 GPa must be done below 200 K in order to prevent the Li diffusing into the diamond anvils of the pressure cell and causing their failure.[50] Using this technique, Li was found to transform first to an intermediate rhombohedral phase (Li-III) at 39 GPa and then to a 16-atom body-centred cubic structure (Li-IV) at 42 GPa.[50] The Li-IV structure (Section 2.3 and Fig. 9) can be regarded as an end-member of the family of modulated layer structures observed in Rb, Cs and Ga at high pressure (Section 2.3). Spectroscopic studies suggest that there are two further transitions near 55 GPa and 69 GPa,[89] the structures of which remain unknown.

Diffraction studies of sodium have recently been extended to 155 GPa and reveal that the *fcc* structure transforms to Na-III with the Li-IV structure (Section 2.3) at 103 GPa, and that there are two further transitions at still higher pressures.[87,90] These phases have also been observed in recent study of the melting curve of Na to 130 GPa, which showed that the melting temperature falls to a minimum of 315 K at 120 GPa before rising again.[91]

Potassium has long been known to have a transition at 23 GPa from the *fcc* K-II phase to the K-III phase which is stable to at least 51 GPa.[53,92,93] Recent angle-dispersive powder studies show K-III to have a composite host–guest structure (see 2.1) comprising a 16-atom tetragonal host structure and a face-centred guest.[94] This is the same structure as that of Rb-IV except that the Rb-IV guest component is body-centred. The superspace group of K-III is $I4/mcm(00q_3)000s$ with lattice parameters a_H = 9.767(1) Å, c_H = 4.732(1) Å, c_G = 2.952(2) Å, $q_3 = c_H/c_G$ = 1.603(2) at 22.1 GPa, and host and guest atoms at (0.7897(3), 0.0847(3), ½) and (½,0,0), respectively.[94] This form of the structure is stable to 31 GPa, where changes in the diffraction pattern may suggest a possible rearrangement of the atoms in the guest chains, but this is not yet known.

The *fcc* phase of Rb, Rb-II, is stable to ~14 GPa[53,92] where it transforms to the *C*-face centred orthorhombic Rb-III (Section 2.3).[19] On further compression to 16.6 GPa, Rb-III transforms to the host–guest composite structure (Section 2.1), Rb-IV,[32] the structural parameters of which at 16.8 GPa are a_H = 10.3503(1) Å, c_H = 5.1865(2) Å, c_G = 3.1797(6) Å, $q_3 = c_H/c_G$ = 1.631(2) with host and guest atoms at (0.7903(1), 0.0851(1), ½) and (½,0,0), respectively.[32] At 19.6(2) GPa, Rb-IV transforms to tetragonal Rb-V,[53,32] which is isostructural with Cs-IV (see 2.4.1).[53] Further compression leads to a transition to orthorhombic Rb-VI at 48.5 GPa,[96] which is isostructural with Cs-V (see 2.4.2) There have been no reported structural studies of Rb above 50 GPa.

An intriguing phenomenon has been found on decreasing the pressure on the Rb-IV phase below 16.7 GPa. The peaks arising from the guest-atom chains of the composite structure broaden significantly, signifying a reduction in the inter-chain coherence length, or a "melting" of the chains.[95] At 16.2 GPa, just above where Rb-IV transforms back to Rb-III at room temperature, the interchain coherence length is only ~30 Å, or 4 times the interchain distance.[95] We have recently made a detailed study of the diffuse scattering from Rb-IV,[97] and have obtained information on the correlation lengths within the guest chains, and the speed of sound along them. The form of the diffuse scattering below 16.7 GPa supports the conclusion that the chains are becoming increasingly 1-D liquid-like as the pressure decreases.[97]

The *fcc* phase of Cs, Cs-II, transforms at 4.2 GPa to Cs-III, which was reported also to be *fcc*.[88] The Cs-II → Cs-III transition was therefore long regarded as one of only two known isostructural transitions in the elements—the other being in cerium.[2] However, new diffraction data appeared inconsistent with *fcc*,[98] and the structure was determined by our own group, using single-crystal techniques, to be *C*-face centred orthorhombic with 84 atoms in the unit cell at 4.3 GPa (Section 2.3 and Fig. 7a).[18] This structure bears no apparent relationship to *fcc* and is it is not clear how the initial diffraction data were obtained. They were collected from a sample in a large-volume device, but when our experiment was repeated under the same conditions, in a similar device, the diffraction pattern obtained was again that of the 84-atom structure.[18] Cs-III is stable over only a very narrow pressure range and transforms at 4.4 GPa to Cs-IV, which is tetragonal and isostructural with Rb-V (see 2.4.1 and Fig. 10).[52] Diffraction studies on Cs have now been extended to 184 GPa.[99] Cs-IV transforms at 10 GPa to orthorhombic Cs-V (see 2.4.2 and Fig. 11)—isostructural with Rb-VI and Si-VI[54]—which in turn transforms to Cs-VI at 72 GPa.[100] Cs-VI is double-hexagonal-close-packed (*dhcp*),[99,100] with a = 3.011(7) Å and c = 9.710(32) Å at 92 GPa, with an axial ratio ($c/2a$ = 1.612(9)) close to that for the ideal close-packing of spheres (1.633). The *dhcp* phase is stable up to 184 GPa, the highest pressure to which Cs has been studied.[99]

3.2 Group 2 (Be, Mg, Ca, Sr, Ba)

Both Be and Mg adopt the *hcp* structure at ambient conditions, with lattice parameters a = 2.2857(4) Å, c = 3.5839(9) Å and c/a = 1.5680(4), and a = 3.2093(3) Å, c = 5.2107(5) Å and c/a = 1.6236(2) respectively.[2] Be maintains this structure up to 171 GPa, the highest pressure at which any of the group 2 metals has been studied,[101] and where the c/a ratio is increased

to 1.609.[101] The *hcp* phase of Mg transforms to *bcc* at ~50 GPa, with a = 2.953(2) Å at 58 GPa.[102] No further transitions are known in Mg up to 70 GPa.[103]

Ca-I has the *fcc* structure at ambient pressure, with a = 5.588(10) Å,[2] and transforms to the Ca-II *bcc* structure at 19.5 GPa.[80] The lattice parameter of the *bcc* phase at 26.5 GPa is a = 3.559(2) Å.[80] Further compression leads to a transition at 32 GPa to Ca-III which has a primitive cubic structure with a = 2.615(2) Å at 39 GPa.[80] This rarely-observed structure (see 2.4.23) is stable over a remarkably wide pressure range, and eventually undergoes a transition to a new phase, Ca-IV, at 113 GPa.[104] Ca-IV has an apparently complex structure which has not yet been solved. At 139 GPa, the appearance of a new Bragg peak may suggest a further phase transition at that pressure.[104]

Sr-I also has the *fcc* structure at ambient pressure, with a = 6.086(2) Å,[2] and transforms to the *bcc* Sr-II structure at 3.5 GPa,[80,105] with a = 4.434(20) Å at 4.2 GPa,[105] and then to the Sr-III phase at ~26 GPa.[80] Sr-III was originally proposed to be orthorhombic[106] but our full 2-D powder-diffraction data revealed that two different phases form at the Sr-II to Sr-III transition—the equilibrium Sr-III phase, with powder lines similar in appearance to those of Sr-II, and another phase, labelled *S*, giving very smooth powder lines.[58] Sr-III was shown to have the tetragonal β-tin structure (see 2.4.3)[58] with a = 5.504(1) Å and c = 2.960(1) Å at 34.8 GPa. On further compression, Sr-III transforms at 35 GPa to Sr-IV which has a body-centred monoclinic structure that is a helical distortion of the Sr-III β-tin structure and is unique to Sr-IV (see 2.4.4. and Fig. 12).[60] Sr-IV is stable from 37.7(2) GPa to 46.3(3) GPa, where it transforms to the incommensurate composite Sr-V phase[31] with superspace group $I4/mcm(00q_3)0000$ (see 2.1). The lattice parameters at 56 GPa are a_H = 6.958(2) Å, c_H = 3.959(2) Å, c_G = 2.820(1) Å and q_3 = 1.404(1), with the host and guest atoms at (x = 0.1460(2), x + ½,0) and (0,0,0), respectively.[31] Additional weak peaks are observed above 71(1) GPa, accompanied by a reduction in the intensity of the guest phase peaks, suggesting a transition in the guest phase structure at this pressure.[31] The structure of this new form is unknown. The smooth minority *S* phase that appears at the Sr-II to Sr-III transition persists unchanged through the transitions to 57 GPa.[60] This and the behaviour of some weak peaks in a narrow pressure range at the transition from Sr-III to Sr-IV remain to be explained.[58,60]

At ambient pressure Ba-I has the *bcc* structure with a = 5.023(2) Å,[2] and this transforms to the *hcp* Ba-II structure at 5.5 GPa, with a = 3.8513(2) Å and c = 5.9729(4) Å, and c/a = 1.5509(1) at 6.9 GPa.[107] The c/a ratio of the *hcp* phase is far from the ideal value of 1.633, and approaches 1.500 at the transition to Ba-IV at 12.6 GPa.[30,107] Ba-IV was the first high-pressure elemental phase found to have a host–guest composite structure (see 2.1 and Fig. 2), and it exhibits a number of different composite forms between 12 and 45 GPa.[30] Between 12.0 and 12.6 GPa, in Ba-IVa, diffraction profiles comprise reflections from two coexisting composite structures with superspace groups $I4/mcm(00q_3)0000$ and $I2/c(q_10q_3)00$. As discussed in Section 2.1, the guest component has a structure that is tetragonal in the former case and monoclinic in the latter. Repeated cycling through the transition from the *hcp* Ba-II phase tends to increase the proportion of the monoclinic form at the expense of the tetragonal one. This and the sharper diffraction peaks of the monoclinic form suggest it is the equilibrium state.[30] On pressure increase above 12.6 GPa, changes in the diffraction peaks arising from the monoclinic guest structure show that it has transformed to an orthorhombic form, Ba-IVb. The structure of this form has yet to be fully determined, but it is clearly another rearrangement of the c-axis guest chains. (The fact that the tetragonal guest is unchanged at this transition supports the conclusion that it is a non-equilibrium form.) On further compression, the c/a ratio of the host unit cell decreases, and at 17.5 GPa has the commensurate value of 1.333 (4/3) at the transition to a different form, Ba-IVd. There is also evidence of an intermediate phase (Ba-IVc) between 16.5 and 17.5 GPa. The next reported transition is to Ba-V at 45 GPa,[107] the structure of which is *hcp* with a = 3.1035(6) Å and c = 4.8778(21) Å at 53 GPa.[107] Although Ba-II and Ba-V both have the *hcp* structure, the c/a ratios of the two structures are quite different: c/a = 1.5717(7) in Ba-V at 53 GPa while in Ba-II at 11.4 GPa, c/a = 1.4984(4).[107] The c/a ratio of Ba-V is also almost pressure independent, while that of Ba-II decreases strongly on compression. These differences suggests that the two *hcp* phases have different bonding characteristics and are different crystallographic phases.[107] However, preliminary studies of the Ba P–T phase diagram,[108] suggest that the stability ranges of Ba-II and Ba-IV may join at high temperatures.

3.3 Group 3 (Sc, Y, La)

Sc, Y and La are the first elements to have a 3*d*, 4*d* and 5*d* electron, respectively, and they are conventionally grouped together with the lanthanide elements due to the similarities in their outer electron configurations and in many of their physical and chemical properties. Y and La have structures and transitions like those of other lanthanide elements and, for this reason, we omit the details here as discussed in Section 1.

Sc has the *hcp* structure at ambient conditions with a = 3.3088(2) Å and c = 5.2675(6) Å[2] and has long been known not to follow the structural sequence of Y, La and the other lanthanide elements. On compression, the *hcp* phase transforms at 20 GPa to Sc-II[109,110] the structure of which was not completely determined[109,110] but was clearly not like any observed in the other lanthanide elements. Recently, using angle-dispersive techniques, structural studies have been extended to 297 GPa.[61] These showed Sc-II to have an incommensurate composite structure that was reported to be isostructural with Bi-III (see 2.1).[111] But more recently we have shown that the guest structure is *C*-centred rather than body-centred, and is thus isostructural with Sr-V.[36] Sc-II then has superspace group $I4/mcm(00q_3)0000$, and the best-fitting parameters at 23 GPa are a_H = 7.5672(1) Å, c_H = 3.4398(1) Å, c_G = 2.6865(1) Å, and $q_3 = c_H/c_G$ = 1.2804(3), with the host and guest atoms at (x = 0.1490(2),x + ½,0) and (0,0,0), respectively.[36] Sc-II transforms to Sc-III at 104 GPa, to Sc-IV at 140 GPa and to Sc-V at 240 GPa.[61] The Sc-IV to Sc-V phase transition is one of only two yet known in the elements at pressures above 200 GPa, the other being in P at 262 GPa.[112]

The structures of Sc-III and Sc-IV are currently unknown, but Sc-V has a hexagonal structure comprising helical chains that is unique to this phase, and which can be regarded as a distortion of the *fcc* structure (see 2.4.5 and Fig. 13).[61]

3.4 Group 4 (Ti, Zr, Hf)

All three of the group 4 elements have the *hcp* structure at ambient conditions, with a = 2.9503(7) Å and c = 4.6836(9) Å in Ti, a = 3.2317(5) Å and c = 5.1476(1) Å in Zr, and a = 3.1940 Å and c = 5.0511 Å in Hf.[2] On compression, all transform to the hexagonal ω-phase—at 7–9 GPa in Ti,[65,66] at 6.7 GPa in Zr,[63] and over the pressure range 45.8–58.3 GPa in Hf.[64] The ω-phase can be regarded as a hexagonal distortion of *bcc* (see 2.4.6).[2] On further compression, both Zr and Hf transform to the *bcc* structure at ~32 GPa in Zr[63,114] and over the pressure range 71.5–78.4 GPa in Hf.[64] The lattice parameters of the *bcc* phases have not been reported.

The *bcc* phase of Hf is stable to at least 252 GPa, the highest pressure at which it has been studied,[64] while the *bcc* phase of Zr has a volume anomaly at ~56 GPa which may mark an isostructural phase transition to another *bcc* phase[63] which is stable to at least 68 GPa. If this isostructural transition is confirmed, it will join the *fcc* to *fcc* transition in Ce in being one of only two such transitions in the elements.[2]

The high-pressure behaviour of Ti is more complex than that of the heavier members of the group.[65,66,115,116] ω-Ti is stable to 116(4) GPa, where it transforms to γ-Ti[65] which has a *C*-face-centred orthorhombic structure (see 2.4.7 and Fig. 14a), space group *Cmcm*, that can be regarded as a distortion of the *bcc* structure.[65,115] On further compression γ-Ti transforms to δ-Ti at 140 GPa,[66,115] which also has a *C*-face-centred orthorhombic structure and space group *Cmcm* like γ-Ti, but which can be regarded as a distortion of the *hcp* rather than *bcc* structure (see 2.4.8 and Fig. 14b).[115] δ-Ti is stable to at least 220 GPa.[66,115] Most recently, it has been reported[116] that a *bcc* phase, which was not observed in Refs 65, 66 and 115, coexists with the ω-phase over the pressure range 40–80 GPa, with the lattice parameter of the *bcc* phase being 2.809(1) Å at 81 GPa.[116]

3.5 Group 5 (V, Nb, Ta)

All three of the group 5 elements have the *bcc* structure at ambient conditions with a = 3.0238(4) Å for V, 3.3007(3) Å for Nb, and 3.3031(6) Å for Ta.[2] No structural transitions are observed up to at least 154 GPa in V and Nb[117] and up to 174 GPa in Ta.[118]

3.6 Group 6 (Cr, Mo, W)

All three of the group 6 elements have the *bcc* structure at ambient conditions with a = 2.8847(5) Å for Cr, 3.1470(3) Å for Mo, and 3.1651(3) Å for W.[2] No structural transitions are observed up to at least 10 GPa in Cr,[119] 272 GPa in Mo[120] and up to 364 GPa in W.[121]

3.7 Group 7 (Mn, Tc, Re)

At ambient conditions, Mn has the complex cubic α-Mn structure (see 2.4.9) which is unique to this element.[2] Perhaps surprisingly in light of the complex nature of this structure, it is stable to 165 GPa, where the appearance of a single additional diffraction peak suggests a transition to a new phase, the structure of which is unknown.[122] Tc has the *hcp* structure at ambient pressure with a = 2.738(3) Å and c = 4.394(5) Å.[145] It is an unstable element and does not exist in nature. No transitions are known to 10 GPa[123] and there have been no high-pressure diffraction studies reported. Re has the *hcp* structure at ambient pressure with a = 2.7608(6) Å and c = 4.4580(5) Å.[2] No phase transitions are observed up to at least 251 GPa.[124,125]

3.8 Group 8 (Fe, Ru, Os)

At ambient conditions, Fe has the *bcc* structure with a = 2.8664(2) Å,[2] and this is stable to 13 GPa where it transforms to the *hcp* structure[126,127] with a = 2.453 Å and c = 3.932 Å at 18.3 GPa.[128] The *hcp* phase is stable to at least 304 GPa.[129] Because of its geophysical importance, the structures and melting curve of Fe have been studied extensively at high pressures and high temperatures. The interested reader is directed to both Tonkov and Ponyatovsky's recent detailed review of the elements[22] and to a recent review on *in situ* studies of Fe.[130]

Both Ru and Os have the *hcp* structure at ambient conditions, with a = 2.7053(8) Å and c = 4.2814(5) Å for Ru, and a = 2.7348(9) Å and c = 4.3193(6) Å for Os.[2] No phase transitions are observed up to at least 56 GPa in Ru[131] and up to 75 GPa in Os,[131,132] although an anomaly in the compressibility of Os at ~25 GPa may suggest a change in the topology of the Fermi surface at that pressure[132]—but see also the discussion of Zn in Section 3.12.

3.9 Group 9 (Co, Rh, Ir)

At ambient conditions, Co has the *hcp* structure with a = 2.5070(3) Å and c = 4.0698(9) Å.[2] On compression, there is a transition to an *fcc* phase over the extended pressure range of 105–150 GPa, and this phase is stable to at least 202 GPa, where a = 3.093(2) Å.[133] Rh has the *fcc* structure at ambient conditions with a = 3.8032(2) Å,[2] and no phase transitions are known up to ~50 GPa.[134]

Ir has the *fcc* structure at ambient conditions, with a = 3.8391(3) Å.[2] On compression there is a transition at 59 GPa to a 14-layer superstructure of the *hcp* structure with a = 2.60 Å and c = 29.68 Å at 65 GPa.[135] Neither the space group nor the atomic coordinates of this phase, which is unique to Ir, are yet known.

3.10 Group 10 (Ni, Pd, Pt)

Ni, Pd and Pt have the *fcc* structure at ambient conditions, with a = 3.5241(7) Å, 3.8900(7) Å and 3.9233(7) Å, respectively, and Pt has the *fcc* structure with a = 3.9233(7) Å. No phase transitions are observed up to at least 65 GPa in Ni,[12] 77.4 GPa in Pd[136] and 304 GPa in Pt.[129]

3.11 Group 11 (Cu, Ag, Au)

All three of the group 11 elements have the *fcc* structure at ambient conditions with a = 3.6148(3) Å in Cu, 4.0857(2) Å in

Ag, and 4.0782(2) Å in Au.[2] No structural transitions are observed up to at least 188 GPa in Cu,[137] 91.8 GPa in Ag[136] and 182 GPa in Au.[137]

3.12 Group 12 (Zn, Cd, Hg)

Both Zn and Cd have the *hcp* structure at ambient conditions, with a = 2.6644(3) Å and c = 4.9454(3) Å for Zn, and a = 2.9788(4) Å and c = 5.6164(6) Å for Cd.[2] The c/a ratios have very non-ideal values of 1.8561(2) and 1.8855(3), respectively. Although no structural transitions are observed up to at least 126 GPa in Zn and 174 GPa in Cd,[138] early diffraction studies reported anomalies in the pressure dependence of the c/a ratio at $\sim$7 GPa and $\sim$10 GPa, respectively, when the c/a ratio passed through the value of $\sqrt{3}$ (1.732).[138–140] It was suggested that these arose from a change in the topology of the Fermi surface.[141] However, not all studies observed such anomalies,[142] and most recently they have been shown to result, at least in Zn, from the effects of a non-hydrostatic medium.[143,144]

Mercury is a liquid at ambient conditions but crystallises into the rhombohedral α-Hg structure on compression to 1.2 GPa (see 2.4.10).[145] On further compression, α-Hg transforms to the body-centred tetragonal β-Hg form at 3.4 GPa (see 2.4.11),[145] which in turn transforms to γ-Hg at 12(2) GPa (see 2.4.12) and then to δ-Hg at $\sim$40 GPa.[146] The δ-Hg phase is stable to at least 67 GPa.[142] The structure of γ-Hg is orthorhombic, but the space group is unknown, while δ-Hg has the *hcp* structure.[146]

3.13 Group 13 (Al, Ga, In, Tl)

Al has the *fcc* structure at ambient conditions with a = 4.0495(1) Å,[2] and initial compression studies showed this phase to be stable to 220 GPa.[147] However, very recently, studies to 333 GPa have reported a transition to an *hcp* structure at 217(10) GPa, with a = 2.2253(9) Å and c = 3.607(3) Å at 292 GPa.[148]

Ga exhibits unusual complexity in its crystal structures, phase transitions, and phase diagram.[2] The ambient-pressure phase, Ga-I, has a unique orthorhombic structure that can be described as made up of Ga_2 dimers (see 2.4.13). On compression at room temperature, this phase melts at 0.5 GPa and then, on further compression, crystallizes at 2 GPa into metastable Ga-III,[149,150] which has the body-centred tetragonal In-I structure (see 2.4.15 and Fig. 16)[51,72] with lattice parameters a = 2.813(3) Å and c = 4.452(5) Å at 2.8 GPa.[51] The stable phase under these conditions, Ga-II, is obtained if Ga-I is compressed through the solid–solid transition below the minimum in the melting temperature at 273 K,[149,150] or if metastable Ga-III is supercooled down to 200 K at pressures around 3 GPa.[51] Ga-II was long believed to have a body-centered cubic structure, space group $I\bar{4}3d$,[51] but subsequent powder diffraction studies were unable to confirm this.[151] Using single-crystal techniques, we have recently shown Ga-II to have a *C*-face-centred orthorhombic structure with 104 atoms per unit cell, that is a modulated layer structure like that observed in Cs-III and Rb-III (see 2.3 and Fig. 8).[49] The previous interpretation in terms of a cubic structure with a much smaller unit cell can be understood on the basis of strong modulation of reflection intensities giving a cubic-like arrangement of clusters of reflections that were probably not resolved as such.[49] On further slow pressure increase of Ga-II we have observed a previously unreported phase transition at 10.5(5) GPa into rhombohedral Ga-V (see 2.4.14 and Fig. 15), which on further compression transforms to the equilibrium Ga-III phase at 14.0(5) GPa.[49] The c/a ratio of Ga-III, which is 1.583(2) at 2.8 GPa[51,72] and 1.5793(9) at 4.0(1) GPa,[49] approaches a value of $\sqrt{2}$ (1.414) on further compression, and there is a continuous transition to the *fcc* Ga-IV structure near 70 GPa.[151] Further studies have confirmed this transition to the *fcc* structure, but have revised the transition pressure significantly to 120(10) GPa.[152] Ga-IV is stable to at least 150 GPa.[152]

In-I has a body-centred tetragonal structure at ambient conditions and is isostructural with Ga-III (see 2.4.15 and Fig. 16). The structure has a c/a ratio of 1.5212(3), and is thus only slightly distorted from *fcc* ($c/a = \sqrt{2}$), and this distortion increases with pressure, with c/a reaching a maximum value of 1.543 at 24 GPa before decreasing with further compression.[153,154] In-I starts to transforms to In-II at 45 GPa,[74a,153] although In-I and In-II cannot be differentiated between 49 and 56 GPa.[74a] In-II has an orthorhombic structure (see 2.4.16) and is stable to at least 93 GPa.[74a]

Tl has an *hcp* structure at ambient conditions with a = 3.4563(5) Å and c = 5.526(4) Å,[2] and on compression it transforms to the *fcc* Tl-II phase near 3.7 GPa[150] with a = 4.778 Å at 6 GPa.[155] This is stable to at least 68 GPa.[151]

3.14 Group 14 (Sn, Pb)

At ambient pressure, Sn has the cubic diamond α-Sn structure below 291 K with a = 6.4892 Å, and the tetragonal β-Sn structure (see 2.4.3) with a = 5.8316(2) Å and c = 3.1815(2) Å above that temperature.[2] On compression, a transition to the body-centred tetragonal Sn-III phase with two atoms per unit cell is observed at 9.2 GPa.[73] This structure has a = 3.70(1) Å and c = 3.37(1) Å at 9.8 GPa, and the c/a ratio of 0.911(4) is only slightly distorted from *bcc* (see 2.4.15). On further compression, the c/a ratio approaches unity,[156] and there is a sluggish transition to the *bcc* structure at 40–50 GPa,[156–158] which is stable up to at least 120 GPa.[158] The lattice parameter of the *bcc* phase at 112 GPa is a = 3.110 Å.[158]

Pb has the *fcc* structure at ambient conditions with a = 4.9502(5) Å,[2] and on compression transforms to the *hcp* structure at 13(1) GPa[159] with a = 3.265(4) Å and c = 5.387(7) Å at 13.9 GPa.[159] This is stable to 111 GPa, where the *hcp* phase transforms to a *bcc* phase which is stable to at least 208 GPa.[160] The lattice parameter of the *bcc* phase at 164 GPa is a = 3.124(10) Å.[160]

3.15 Group 15 (As, Sb, Bi)

Although group 15 elements, especially Bi, have long attracted the attention of those studying the high-pressure behaviour of the elements, it is only in the last 5–6 years that their true behaviour at high pressure has been clarified. The high-pressure behaviour of these elements has recently been reviewed in detail.[40]

At ambient conditions, As-I, Sb-I and Bi-I all adopt the trigonal As-I structure (see 2.4.17). On pressure increase, Bi-I transforms at 2.55 GPa to *C*-face-centred monoclinic Bi-II, the structure of which is unique to Bi-II (see 2.4.18 and Fig. 17).[75] At 2.7 GPa, Bi-II transforms to Bi-III. The Bi-III structure has been the subject of uncertainty since the 1930's, although numerous solutions have been proposed, as reviewed in Ref 40. Much of this uncertainty was caused by the tendency for Bi to recrystallise on passing through the Bi-II→Bi-III transition, leading to highly textured samples of Bi-III. However, by utilising this recrystallisation to obtain a quasi-single crystal of Bi-III, and also making high-quality powdered samples by passing through the Bi-II→Bi-III transition at low temperatures (200 K), we were able to show that Bi-III has an incommensurate composite structure, superspace group $I'4/mcm(00q_3)0000$ (see 2.1).[162] The lattice parameters at 6.8 GPa are a_H = 8.5182(2) Å, c_H = 4.1642(2) Å and c_G = 3.1800(3), and $q_3 = c_H/c_G$ = 1.309(1), with host and guest atoms at (x = 0.1536(3),x + ½,0) and (0,0,0), respectively.[161] Bi-III was the first composite structure found in the elements outwith the group 1 and 2 elements. As well as accounting for the complex diffraction pattern of Bi-III, the non-integer number of atoms in the composite unit cell also resolved the longstanding problem of its calculated density, which now agrees extremely well with the measurement of Bridgman (see 2.1). Bi-III is stable to 7.7 GPa where it transforms to the *bcc* structure of Bi-V, which is stable to at least 222 GPa.[162] The lattice parameter of the *bcc* phase at 9.7 GPa is 3.781(1) Å.[161]

Sb-I has long been reported to transform to Sb-II at ~8.6 GPa (but see Sb-IV below), diffraction patterns from which were known to be similar to those of Bi-III.[40] And Sb-II has been shown to have the same incommensurate composite structure as Bi-III, with the same $I'4/mcm(00q_3)0000$ superspace group. It has a_H = 8.0751(7) Å, c_H = 3.9120(5) Å, c_G = 2.9856(8) Å, and $q_3 = c_H/c_G$ = 1.310(1) at 10.3 GPa.[37,163] The refined atomic coordinates of the host and guest atoms at the same pressure are (x = 0.1558(4), x + ½,0) and (0,0,0), respectively. On pressure increase, Sb-II is stable to 28 GPa where it transforms to Sb-III which has the *bcc* structure.[164] This is stable to at least 43 GPa.[164]

We have recently identified a new phase of antimony, Sb-IV, existing between Sb-I and Sb-II.[35] This phase is observed from 8.2 and 9.0 GPa on pressure increase and between 8 and 6.9 GPa on pressure decrease.[35] Sb-IV has a monoclinic composite structure, superspace group $I2/c(q_10q_3)00$, with a_H = 8.1710(2) Å, b_H = 8.1616(2) Å, c_H = 3.9504(1) Å, β_H = 89.456(1)°, a_G = 8.1815(2) Å, $b_G = b_H$, c_G = 3.0083(1) Å, β_G = 92.959(1)°, q_1 = 0.1662(1) and q_3 = 1.3132(1) at 6.9 GPa (see Section 2.1).[35] The atomic coordinates of the host and guest atoms at the same pressure are (0.1611(4), 0.6569(3), 0.004(1)) and (0,0,0), respectively. The monoclinic symmetry allows the guest atoms to form zig-zag chains, and Sb-IV is thus the first host–guest phase observed to have non-linear guest atom chains.[35]

As described in 2.4.17, the ambient-pressure phases of As, Sb and Bi can all be regarded as distortions of the primitive cubic structure. While this distortion decreases in Sb-I and Bi-I on compression, transitions to Sb-II and Bi-II occur before the primitive cubic phase is found. However, a primitive cubic phase of As, As-II, is found on compression to 25(1) GPa.[165,166] This joins α-Po and Ca-III as the known examples of a simple cubic phase in the elements (see 2.4.23). The lattice parameter of the primitive cubic structure at 25 GPa is 2.550(4) Å.[166] As-II is stable until ~46 GPa where it transforms to As-III.[167] which has a monoclinic incommensurate composite structure with superspace group $I2/c(q_10q_3)00$, and is thus isostructural with Sb-IV rather than Sb-II and Bi-III (see 2.1).[165] The structural parameters at 50 GPa are a_H = 6.7673(2) Å, b_H = 6.7464(2) Å, c_H = 3.2491(1) Å, β_H = 89.654(2)°, a_G = 6.7719(2) Å, $b_G = b_H$, c_G = 2.4903(1) Å and β_G = 92.099(2)°.[37] The modulation vector at the same pressure has q_1 = 0.1162(3) and q_3 = 1.3047(1), and the host and guest atoms are at (0.1612(5), 0.6521(5), −0.004(2)) and (0,0,0), respectively.[37] As-III is stable to ~110 GPa where it transforms to As-IV which has the *bcc* structure.[167] This phase is stable to at least 122 GPa where the lattice parameter is a = 2.806 Å.[167]

3.16 Group 16 (S, Se, Te, Po)

Recent diffraction studies of S, Se and Te have rewritten most of what was previously known about these elements at high-pressure. Although not a metal at ambient conditions, sulfur becomes metallic above 95 GPa,[168] and we have therefore included it for completeness.

At ambient conditions, Se and Te both have the trigonal Se-I structure (see 2.4.21).[2] Te has attracted the most attention of the group 16 elements at high pressure, probably because it has the lowest transition pressures. Despite numerous studies,[22] however, it is only recently that the structures of its high-pressure phases have been determined definitively.[20,78,84] Trigonal Te-I transforms to Te-II at 4 GPa (see 2.4.22 and Fig. 19). This was initially reported to be monoclinic,[169] but our recent studies have revealed a wealth of additional weak reflections that show the structure to be triclinic, one of the very few examples of this symmetry in the elements (see 2.4.22).[78] We adopted a non-standard body-centered triclinic setting, space group $I\bar{1}$, to aid comparison with the Te-III structure. The transition from Te-II to Te-III starts at 4.5(2) GPa, but the two phases coexist over a wide pressure range.[78,20] Te-III is incommensurate, superspace group $I'2/m(0q_20)s0$, where $(0q_20)$ is the wavevector of the incommensurate modulation, and was only the third incommensurate modulated phase found in the elements after uranium (see 2.2 and Fig. 4) and iodine.[44] The identification of the structure as incommensurate became possible after a quasi-single crystal of Te-III was obtained at 7.4 GPa and clearly revealed the presence of satellite peaks around the main reflections (see 2.2 and Fig. 5 and 6). On compression the Te-III structure approaches that of the rhombohedral β-Po structure (see Fig. 20 and 2.4.24), but at 29.2(7) GPa it transforms directly to *bcc* Te-V[20] which is stable to at least 37 GPa.[170] The lattice parameter of Te-V at 35.9 GPa is 3.4414(5) Å.[20] The previously reported Te-IV phase with the β-Po structure is not observed at room temperature, although we have recently observed this phase between the Te-III and Te-V phases at temperatures above 315 K.[84]

At ambient conditions, Se-I has the same trigonal structure as Te-I (see 2.4.21). At 14 GPa, Se-I transforms to Se-II which

is reported to have a C-face-centred monoclinic structure.[171] However, our own recent studies of Se-II, while unable to determine its structure, were able to show that the monoclinic structure is incorrect. Se-II is stable to 22 GPa where it transforms to Se-III, which in turn transforms to Se-IV at 29 GPa.[42] Se-III and Se-IV are isostructural with Te-II and Te-III, respectively.[42,78] The incommensurate wavevector of Se-IV ($0q_20$), is significantly pressure dependent, with q_2 changing from 0.314(1) at 28.9 GPa to 0.277(1) at 56 GPa.[42] Se-IV is stable to approximately 80 GPa,[85] where it transforms to Se-V with the rhombohedral β-Po structure (see 2.4.24). This is stable to 140(3) GPa, where it transforms to Se-VI with the *bcc* structure.[83,85] The lattice parameter of the *bcc* phase at 140 GPa is a = 2.823(1) Å.[83]

Sulfur exists in a large number of complex allotropic forms at ambient conditions, and numerous high-pressure forms have also been reported.[2,22] The stable crystal structure at ambient conditions (see 2.4.19) comprises covalently-bonded S_8 rings arranged in an orthorhombic structure, space group *Fddd*.[2] On compression at room temperature, this orthorhombic form was reported to undergo a gradual transition to an amorphous form at 26 GPa,[172] which then began to recrystallise at 37 GPa.[173,176] The structure of this recrystallized form, named S-II, has recently been shown to have a body-centered tetragonal structure, space group $I4_1/acd$, comprising parallel chains of atoms with 4_1 and 4_3 screw-axis symmetry running along the c-axis (see 2.4.20 and Fig. 18).[174,175] The lattice parameters of S-II at 55 GPa are a = 7.841(1) Å and c = 3.100(1) Å.[174] A further phase transition, to S-III, occurs on compression to 83–86 GPa,[176] and S-III is both metallic and superconducting. We have recently shown S-III to be incommensurately modulated, and isostructural with Te-III and Se-IV (see 2.2).[43,85] Sulfur was the first element observed to have an incommensurate structure above 100 GPa. On further pressure increase, the modulated phase transforms to the rhombohedral β-Po structure (see Fig. 20 and 2.4.24) at 150–160 GPa,[173] and this phase is stable to at least 212 GPa.[173] On pressure decrease at 90 GPa, a triclinic phase, S-V, is observed, which is isostructural with triclinic Se-IV and Te-II.[43]

Polonium has a primitive cubic structure at ambient conditions (see 2.4.23) with a = 3.352 Å at 283 K.[2] There have been no reported high-pressure studies of Po, and nothing is known about its high-pressure behaviour.

4. Discussion and conclusions

A comparison of the monographs by Young in 1991,[12] and Tonkov and Ponyatovsky in 2005[22] reveals the remarkable progress that has been made in determining the high-pressure structural behaviour of the elements over the last 15 years. Much, if not all, of this progress can be attributed to the development of angle-dispersive powder diffraction techniques in the early 1990's, the opening of third-generation synchrotron sources in the mid 1990's, and the development of single-crystal techniques using CCD 2-D detectors at the end of that decade. The ability to obtain high-resolution powder-diffraction profiles free of contamination from fluorescence peaks, and with full-pattern integration giving peak intensities accurate enough to make full Rietveld refinement possible, opened the way to determining the structures of low-symmetry structures at high pressure for the first time, and for refining their structural parameters. The advent of third-generation synchrotron sources, with their extremely intense beams of high-energy X-rays, enabled detailed structural studies of complex phases to be obtained from weakly scattering elements, and their study to be extended to pressures above 200 GPa. And the recent development of single-crystal methods has made possible the identification and determination of high-pressure incommensurate structures for the first time, the solution of which would have defeated standard powder methods.

The key feature of these studies of the metallic elements is the complexity of the new structures that have been observed. Of the 18 different crystal structures discovered in the elements since 1990, as described in Sections 2 and 3, only two—S-II and Sc-V (see 2.4.5 and 2.4.20)—are commensurate and have a symmetry that is tetragonal or higher. The others are all incommensurate (7), orthorhombic (6), rhombohedral (1), monoclinic (1) or triclinic (1). And, in all but incommensurate Te-III, the structures have at least one variable atomic coordinate. Thus, while the majority of the metallic elements have high-symmetry structures at ambient conditions (Section 3), pressure induces transitions to a variety of low-symmetry structures, and a diversity of behaviour that is considerably greater than that observed at ambient pressure.

The most notable difference between the ambient and high-pressure structures of the elements is the widespread existence of incommensurate structures at high pressures. As said in Section 2, prior to 1999 the only element reported to have an incommensurately modulated structure was the low-temperature charge-density-wave state of uranium. Since then, the discovery of incommensurate composite structures in the group 1, 2, 3 and 15 elements and phase transitions between such structures, and the discovery of strongly modulated incommensurate structures in the group 16 and 17 elements, have shown that such structures are not only widely observed, but that they are stable over wide ranges of pressure and temperature. For example, Se-IV is stable over a pressure range of 40 GPa, S-III over a pressure range of ~70 GPa, and Ba-IV is stable over 33 GPa and to at least 700 K. Thirteen elements, as shown in Fig. 21, are now known to be incommensurate at high pressures, and in three more—Na, Ca and P[91,104,178,179]—it has been suggested that incommensurate structures may exist. Indeed, in view of the recent discovery of a composite structure in a transition metal (Sc)—and the number of incommensurate phases already observed in the elements in the same columns as Na, Ca and P (Fig. 21)—it would perhaps be surprising if further examples of such structures were not found in these and other elements in the future.

The reasons why such structures should exist at high pressures is still unclear, as the very thing that makes them so interesting, their incommensurate nature, also prevents exact electronic structure calculations of their properties. Such calculations can, however, use commensurate analogues of the incommensurate structures as approximations, and these have provided some insight into the composite structures, and have

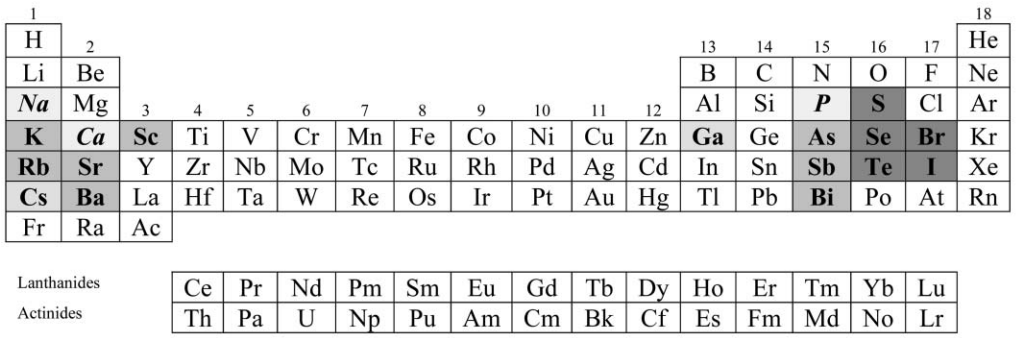

Fig. 21 The periodic table, showing elements so far found to have incommensurate and modulated high-pressure phases. Those shaded in light grey have modulated layer structures (Section 2.3) but are not known to have incommensurate phases (Rb has both). Those shaded in medium grey have incommensurate composite structures (Section 2.1). Those shaded in dark grey have incommensurate modulated structures (Section 2.2). There may also be incommensurate structures in those shown in italics—Na, Ca, and P. Groups are numbered at the top of each column.

started to reproduce the reported transition sequence quite well.[180–182] The first calculations of Ba-IV (using a commensurate analogue) suggested that the host and guest atoms had different electronic structures,[180] with the host and guest atoms being more *s* and *d* like, respectively. Such differences were not found in calculations of the composite structures in the group 15 elements, which rather suggested that the stability of the composite structures arises from the delicate interplay of band energy, which would favour open-packed structures, and electrostatic energy, which would favour high-symmetry close-packed structures.[181]

Recent calculations have also given insight into the modulated phase of sulfur. Calculations of the Fermi surface at 100 GPa show that it exhibits parallel zones, indicating Fermi surface nesting, characterised by a wavevector that is very similar to that observed experimentally.[183] And calculations of phonon dispersion at the same pressure show a softening at the same wavevector as the nesting vector. These results indicate that the incommensurate phase in metallic sulfur at megabar pressures—and probably, therefore, in Se-IV and Te-II too—is due to a charge-density wave.

The extreme complexity of some of the non-incommensurate structures has also attracted attention from theorists, in particular the structures of Cs-III, Rb-III and Ga-II, with 84, 52 and 104 atoms per unit cell, respectively. These have recently been analysed within the Hume–Rothery mechanism.[184,185] This suggests that structural distortions give rise to new diffraction planes forming a Brillouin zone (BZ) boundary close to the Fermi surface (FS).[184,185] The resulting interaction between the BZ boundary and the FS then results in the opening of a pseudogap and a reduction in the overall electronic energy of the structure. It has also been suggested that a BZ–FS interaction could account for the incommensurate composite phases.[185] Other studies of the Cs-III, Rb-III and Ga-II structures have focused on the transition paths between the structures[186] or on electron localisation within the 2-D layers forming the structures.[187]

As a result of greatly improved experimental techniques and facilities, the last 15 years has seen many of the outstanding uncertainties in the structures of the elements at high pressure removed. Combined with modern computational methods, much is now understood about the behaviour of elements at high pressure. However, there are still a number of outstanding questions and further studies are needed. Of particular interest would be the discovery of further new incommensurate structures. The recent discovery of a composite structure in Sc (Ref. 36) shows that these structures are no longer confined to groups 1, 2 and 15 of the periodic table, although the current best candidates for further such structures, in Na, Ca and P (see above), are indeed within these groups. There is also a need for high- and low-temperature studies of structural behaviour. Comparatively little is known about the high-pressure structures and transitions of the elements at high, and especially low, temperatures, and it is not certain, therefore, whether the complex behaviour observed at room temperature is maintained under these conditions. In addition, the increasing number of structural studies of high-pressure high-temperature liquids[122,23] means that information on the structures of the crystalline phases below the liquid phase are required both to help interpret diffraction data from the liquid phase, and to determine density changes on melting. And knowledge of structural complexity at low temperatures is required in order to correlate the existence of complex structures with the pressure-induced superconductivity observed in many elements.[3] Structural studies within the superconducting phase are technically challenging, but are possible.

Finally, the difference in the electronic structures in the elements at high pressure signalled by these large changes in structure has led them to be described "new" elements with new chemistry that can be used to create new materials.[188–190] The pioneering work of Badding and coworkers has demonstrated that potassium behaves more like a transition metal at high pressures than an alkali metal, and, as a result, it can form stoichiometric K–Cu and K–Ag alloys that do not form at ambient conditions.[188–190] This field is still in its infancy, but similar behaviour in general at high pressure promises to open the way to wholly new materials with sought after properties.

Acknowledgements

We gratefully acknowledge the contributions of numerous colleagues to the structure determinations from our own group

included in this review, especially D. R. Allan, S. A. Belmonte, J. S. Loveday, T. Bovornratanaraks, O. Degtyareva, S. Rekhi, C. Hejny, S. Falconi and L. F. Lundergaard.

We have also benefited particularly from interactions with V. F. Degtyareva, N. W. Ashcroft, S. van Smaalen, L. Palatinus, V. Petricek, U. Häussermann, K. Syassen, U. Schwarz, M. Hanfland, J. S. Tse, T. R. Welberry, R. A. Cowley and G. J. Ackland. The programme overall has been supported by research grants from the Engineering and Physical Sciences Research Council (EPSRC). The technical developments and research at SRS Daresbury Laboratory has also been supported by funding from the Council for the Central Laboratory of the Research Councils (CCLRC), and by facilities made available by Daresbury Laboratory. We thank G. Bushnell-Wye, S. Teat, M. Roberts, A. Lennie, J. Maclean and T. Prior for support in the maintenance and use of SRS beamlines. We are also grateful to M. Hanfland, W. Crichton and M. Mezouar for their support in using beamline facilities at ESRF, and for the encouragement of ESRF in developing single-crystal techniques further. For part of the period of our own work covered in the review, one of us (MIM) was supported by a Royal Society University Research Fellowship.

References

1 P. W. Bridgman, *Collected Experimental Papers*, Harvard University Press, Cambridge, MA, USA, 1964.
2 J. Donohue, *The Structure of the Elements*, Robert E. Krieger Publishing Company, Malabar, FL, 1982.
3 C. Buzea and K. Robbie, *Supercond. Sci. Technol.*, 2005, **18**, R1–R8.
4 M. I. Eremets, V. V. Struzhkin, H. K. Mao and R. J. Hemley, *Science*, 2001, **293**, 272–274.
5 K. Shimizu, K. Suhara, M. Ikumo, M. I. Eremets and K. Amaya, *Nature*, 1998, **393**, 767–769.
6 V. V. Struzhkin, R. J. Hemley, H. K. Mao and Y. A. Timofeev, *Nature*, 1997, **390**, 382–384.
7 K. Takemura, S. Minomura, O. Shimomura and Y. Fujii, *Phys. Rev. Lett.*, 1980, **45**, 1881–1884.
8 R. M. Hazen, *The Diamond Makers*, Cambridge University Press, Cambridge, UK, 1999.
9 M. I. Eremets, R. J. Hemley, H. K. Mao and E. Gregoryanz, *Nature*, 2001, **411**, 170–174.
10 H. K. Mao and R. J. Hemley, *Rev. Mod. Phys.*, 1994, **66**, 671–692.
11 C. W. F. T. Pistorius, *Prog. Solid State Chem.*, 1976, **11**, 1–151.
12 D. A. Young, *Phase Diagrams of the Elements*, University of California Press, Berkeley, CA, 1991.
13 M. T. Yin and M. L. Cohen, *Phys. Rev. B: Condens. Matter*, 1982, **26**, 5668–5687.
14 M. T. Yin, *Phys. Rev. B: Condens. Matter*, 1984, **30**, 1773–1776.
15 V. K. Fedotov, E. G. Ponyatovskii, V. A. Somenkov and S. Sh. Shil'shtein, *Fiz. Tverd. Tela (Leningrad)*, 1978, **20**, 1088–1096, (*Sov. Phys. Solid State*, 1978, **20**, 1267).
16 O. Shimomura, K. Takemura, H. Fujihisa, Y. Fujii, Y. Ohishi, T. Kikegawa, Y. Amemiya and T. Matsushita, *Rev. Sci. Instrum.*, 1992, **63**, 967–973.
17 R. J. Nelmes and M. I. McMahon, *J. Synchrotron Radiat.*, 1994, **1**, 69–73.
18 M. I. McMahon, R. J. Nelmes and S. Rekhi, *Phys. Rev. Lett.*, 2001, **87**, 255502.
19 R. J. Nelmes, M. I. McMahon, J. S. Loveday and S. Rekhi, *Phys. Rev. Lett.*, 2002, **88**, 155503.
20 C. Hejny and M. I. McMahon, *Phys. Rev. Lett.*, 2003, **91**, 215502.
21 R. M. Martin, *Electronic Structure: Basic Theory and Practical Methods*, Cambridge University Press, Cambridge, UK, 2005.
22 E. Yu Tonkov and E. G. Ponyatovsky, *Phase Transformations of Elements under High Pressure*, CRC Press, Boca Raton, FL, USA, 2005.
23 S. Falconi, L. F. Lundegaard, C. Hejny and M. I. McMahon, *Phys. Rev. Lett.*, 2005, **94**, 125507.
24 N. Funamori and K. Tsuji, *Phys. Rev. B: Condens. Matter Mater. Phys.*, 2002, **65**, 014105.
25 G. Shen, V. B. Prakapenka, M. L. Rivers and S. R. Sutton, *Phys. Rev. Lett.*, 2004, **92**, 185701.
26 G. Monaco, S. Falconi, W. A. Crichton and M. Mezouar, *Phys. Rev. Lett.*, 2003, **90**, 255701.
27 S. Japel, B. Schwager, R. Boehler and M. Ross, *Phys. Rev. Lett.*, 2005, **95**, 167801.
28 R. Boehler, *Rev. Geophys.*, 2000, **38**, 221–245.
29 V. Petricek, K. Maly, P. Coppens, X. Bu, I. Cisarova and A. Frost-Jensen, *Acta Crystallogr., Sect. A: Fundam. Crystallogr.*, 1991, **47**, 210–216.
30 R. J. Nelmes, D. R. Allan, M. I. McMahon and S. A. Belmonte, *Phys. Rev. Lett.*, 1999, **83**, 4081–4084.
31 M. I. McMahon, T. Bovornratanaraks, D. R. Allan, S. A. Belmonte and R. J. Nelmes, *Phys. Rev. B: Condens. Matter Mater. Phys.*, 2000, **61**, 3135–3138.
32 M. I. McMahon, S. Rekhi and R. J. Nelmes, *Phys. Rev. Lett.*, 2001, **87**, 055501.
33 M. I. McMahon, R. J. Nelmes, U. Schwarz and K. Syassen, *Phys. Rev. B: Condens. Matter Mater. Phys.*, submitted.
34 M. I. McMahon, O. Degtyareva and R. J. Nelmes, *Phys. Rev. Lett.*, 2000, **85**, 4896–4899.
35 O. Degtyareva, M. I. McMahon and R. J. Nelmes, *Phys. Rev. B: Condens. Matter Mater. Phys.*, 2004, **70**, 184119.
36 M. I. McMahon, L. F. Lundegaard, C. Hejny, S. Falconi and R. J. Nelmes, *Phys. Rev. B: Condens. Matter Mater. Phys.*, 2006, **73**, 134102.
37 M. I. McMahon and R. J. Nelmes, *Z. Kristallogr.*, 2004, **219**, 742–748.
38 S. van Smaalen, *Cryst. Rev.*, 1995, **4**, 79–202.
39 S. van Smaalen, *Mater. Sci. Forum*, 1992, **100–101**, 173–222.
40 O. Degtyareva, M. I. McMahon and R. J. Nelmes, *High Pressure Res.*, 2004, **24**, 319–356.
41 H. G. Smith and G. H. Lander, *Phys. Rev. B: Condens. Matter*, 1984, **30**, 5407–5415.
42 M. I. McMahon, C. Hejny, J. S. Loveday, L. F. Lundegaard and M. Hanfland, *Phys. Rev. B: Condens. Matter Mater. Phys.*, 2004, **70**, 054101.
43 C. Hejny, L. F. Lundegaard, S. Falconi, M. I. McMahon and M. Hanfland, *Phys. Rev. B: Condens. Matter Mater. Phys.*, 2005, **71**, 020101(R).
44 K. Takemura, K. Sato, H. Fujihisa and M. Onoda, *Nature*, 2003, **423**, 971–974.
45 T. Kume, T. Hiraoka, Y. Ohya, S. Sasaki and H. Shimizu, *Phys. Rev. Lett.*, 2005, **94**, 065506.
46 H. G. Smith and G. H. Lander, *Phys. Rev. B: Condens. Matter*, 1984, **30**, 5407–5415.
47 J. C. Marmeggi, G. H. Lander, S. van Smaalen, T. Brückel and C. M. E. Zeyen, *Phys. Rev. B: Condens. Matter*, 1990, **42**, 9365–9376.
48 R. J. Nelmes, M. I. McMahon, J. S. Loveday and S. Rekhi, *Phys. Rev. Lett.*, 2002, **88**, 155503.
49 O. Degtyareva, M. I. McMahon, D. R. Allan and R. J. Nelmes, *Phys. Rev. Lett.*, 2004, **93**, 205502.
50 M. Hanfland, K. Syassen, N. E. Christensen and D. L. Novikov, *Nature*, 2000, **408**, 174–178.
51 L. Bosio, *J. Chem. Phys.*, 1978, **68**, 1221–1223.
52 K. Takemura, S. Minomura and O. Shimomura, *Phys. Rev. Lett.*, 1982, **49**, 1772–1775.
53 H. Olijnyk and W. B. Holzapfel, *Phys. Lett. A*, 1982, **99**, 381–383.
54 U. Schwarz, K. Takemura, M. Hanfland and K. Syassen, *Phys. Rev. Lett.*, 1998, **81**, 2711–2714.
55 U. Schwarz, K. Syassen, A. Grzechnik and M. Hanfland, *Solid State Commun.*, 1999, **112**, 319–322.
56 M. Hanfland, U. Schwarz, K. Syassen and K. Takemura, *Phys. Rev. Lett.*, 1999, **82**, 1197–1200.
57 K. Takemura, U. Schwarz, K. Syassen, M. Hanfland, N. E. Christensen, D. L. Novikov and I. Loa, *Phys. Rev. B: Condens. Matter Mater. Phys.*, 2000, **62**, R10603–R10606.

58 D. R. Allan, R. J. Nelmes, M. I. McMahon, S. A. Belmonte and T. Bovornratanaraks, *Rev. High Pressure Sci. Technol.*, 1998, **7**, 236–238.
59 R. J. Nelmes and M. I. McMahon, *Semicond. Semimet.*, 1998, **54**, 145–246.
60 T. Bovornratanaraks, D. R. Allan, S. A. Belmonte, M. I. McMahon and R. J. Nelmes, *Phys. Rev. B: Condens. Matter Mater. Phys.*, 2006, **73**, 144112.
61 Y. Akahama, H. Fujihisa and H. Kawamura, *Phys. Rev. Lett.*, 2005, **94**, 195503.
62 J. C. Jamieson, *Science*, 1963, **140**, 72–73.
63 Y. Akahama, M. Kobayashi and H. Kawamura, *J. Phys. Soc. Jpn.*, 1991, **60**, 3211–3214.
64 H. Xia, G. Parthasarathy, H. Luo, Y. K. Vohra and A. L. Ruoff, *Phys. Rev. B: Condens. Matter*, 1990, **42**, 6736–6738.
65 Y. K. Vohra and P. T. Spencer, *Phys. Rev. Lett.*, 2001, **86**, 3068–3071.
66 Y. Akahama, H. Kawamura and T. Le Bihan, *Phys. Rev. Lett.*, 2001, **87**, 275503.
67 T. Yamada and Y. Fujii, *J. Phys. Soc. Jpn.*, 1970, **28**, 1503–1507.
68 W. Klement, Jr., A. Jayaraman and G. C. Kennedy, *Phys. Rev.*, 1963, **131**, 1–6.
69 C. S. Barret, *Acta Crystallogr.*, 1957, **10**, 58–60.
70 M. Atoji, J. E. Schirber and C. A. Swenson, *J. Chem. Phys.*, 1959, **31**, 1628–1629.
71 O. Schulte and W. B. Holzapfel, *Phys. Rev. B: Condens. Matter*, 1993, **48**, 14009–14012.
72 C. E. Weir, G. J. Piermarini and S. Block, *J. Chem. Phys.*, 1971, **54**, 2768–2770.
73 J. D. Barnett, V. E. Dean and H. T. Hall, *J. Appl. Phys.*, 1966, **37**, 875–877.
74 (*a*) K. Takemura and H. Fujihisa, *Phys. Rev. B: Condens. Matter*, 1993, **47**, 8465–8470; (*b*) J. C. Jamieson, *Science*, 1963, **139**, 1291–1292; (*c*) T. Kikegawa and H. Iwasaki, *Acta Crystallogr., Sect. B: Struct. Sci.*, 1983, **39**, 158–164.
75 R. M. Brugger, R. B. Bennion and T. G. Worlton, *Phys. Lett. A*, 1967, **24**, 714–717.
76 S. J. Rettig and J. Trotter, *Acta Crystallogr., Sect. C: Cryst. Struct. Commun.*, 1987, **43**, 2260–2262.
77 H. Fujihisa, Y. Akahama, H. Kawamura, H. Yamawaki, M. Sakashita, T. Yamada, K. Honda and T. Le Bihan, *Phys. Rev. B: Condens. Matter Mater. Phys.*, 2004, **70**, 134106.
78 C. Hejny and M. I. McMahon, *Phys. Rev. B: Condens. Matter Mater. Phys.*, 2004, **70**, 184109.
79 R. B. Roof, Jr., *J. Less-Common Met.*, 1986, **120**, 345–349.
80 H. Olijnyk and W. B. Holzapfel, *Phys. Lett. A*, 1984, **100**, 191–194.
81 T. Kikegawa and H. Iwasaki, *J. Phys. Soc. Jpn.*, 1987, **56**, 3417–3420.
82 H. Luo, R. G. Greene and A. L. Ruoff, *Phys. Rev. Lett.*, 1993, **71**, 2943–2946.
83 Y. Akahama, M. Kobayashi and H. Kawamura, *Phys. Rev. B: Condens. Matter*, 1993, **47**, 20–26.
84 C. Hejny, S. Falconi, L. F. Lundegaard and M. I. McMahon, *Phys. Rev. B: Condens. Matter Mater. Phys.*, submitted.
85 O. Degtyareva, E. Gregoryanz, M. Somayazulu, H. K. Mao and R. J. Hemley, *Phys. Rev. B: Condens. Matter Mater. Phys.*, 2005, **71**, 214104.
86 B. Olinger and W. Shaner, *Science*, 1983, **219**, 1071–1072.
87 M. Hanfland, I. Loa and K. Syassen, *Phys. Rev. B: Condens. Matter Mater. Phys.*, 2002, **65**, 184109.
88 H. T. Hall, L. Merrill and J. D. Barnett, *Science*, 1964, **146**, 1297–1299.
89 A. F. Goncharov, V. V. Struzhkin, H. K. Mao and R. J. Hemley, *Phys. Rev. B: Condens. Matter Mater. Phys.*, 2005, **71**, 184114.
90 K. Syassen, in 40th European High-Pressure Research Group Meeting (Edinburgh, 2002), Abstracts p. 56.
91 E. Gregoryanz, O. Degtyareva, M. Somayazulu, R. J. Hemley and H. K. Mao, *Phys. Rev. Lett.*, 2005, **94**, 185502.
92 M. Winzenick, V. Vijayakumar and W. B. Holzapfel, *Phys. Rev. B: Condens. Matter*, 1994, **50**, 12381–12385.
93 L.-G. Liu, *J. Phys. Chem. Solids*, 1986, **47**, 1067–1072.
94 M. I. McMahon, R. J. Nelmes, U. Schwarz and K. Syassen, *Phys. Rev. B: Condens. Matter Mater. Phys.*, submitted.
95 M. I. McMahon and R. J. Nelmes, *Phys. Rev. Lett.*, 2004, **93**, 055501.
96 U. Schwarz, K. Syassen, A. Grzechnik and M. Hanfland, *Solid State Commun.*, 1999, **112**, 319–322.
97 S. Falconi, M. I. McMahon, L. F. Lundegaard, C. Hejny, R. J. Nelmes and M. Hanfland, *Phys. Rev. B: Condens. Matter Mater. Phys.*, 2006, **93**, 214102.
98 U. Schwarz, K. Takemura, M. Hanfland and K. Syassen, *Phys. Rev. Lett.*, 1998, **81**, 2711–2714.
99 K. Takemura, N. E. Christensen, D. Novikov, K. Syassen, U. Schwarz and M. Hanfland, *Phys. Rev. B: Condens. Matter Mater. Phys.*, 2000, **61**, 14399–14404.
100 K. Takemura, O. Shimomura and H. Fujihisa, *Phys. Rev. Lett.*, 1991, **66**, 2014–2017.
101 K. Nakano, Y. Akahama and H. Kawamura, *J. Phys.: Condens. Matter*, 2002, **14**, 10569–10573.
102 H. Olijnyk and W. B. Holzapfel, *Phys. Rev. B: Condens. Matter*, 1985, **31**, 4682–4683.
103 M. Winzenick and W. B. Holzapfel, in *High Pressure Science and Technology*, ed W. Trzeciakowski, World Sci, Singapore, 1996, pp. 384–386.
104 T. Yabuuchi, Y. Nakamoto, K. Shimizu and T. Kikegawa, *J. Phys. Soc. Jpn.*, 2005, **74**, 2391–2392.
105 D. B. McWhan and A. Jayaraman, *Appl. Phys. Lett.*, 1963, **3**, 129.
106 M. Winzenick and W. B. Holzapfel, *Phys. Rev. B: Condens. Matter*, 1996, **53**, 2151–2154.
107 T. Kenichi, *Phys. Rev. B: Condens. Matter*, 1994, **50**, 16238–16246.
108 M. Winzenick and W. B. Holzapfel, *Phys. Rev. B: Condens. Matter*, 1997, **55**, 101–104.
109 Y. K. Vohra, A. Grosshans and W. B. Holzapfel, *Phys. Rev. B: Condens. Matter*, 1982, **25**, 6019–6021.
110 Y. C. Zhao, F. Porsch and W. B. Holzapfel, *Phys. Rev. B: Condens. Matter*, 1996, **54**, 9715–9720.
111 H. Fujihisa, Y. Akahama, H. Kawamura, Y. Gotoh, H. Yamawaki, M. Sakashita, S. Takeya and K. Honda, *Phys. Rev. B: Condens. Matter Mater. Phys.*, 2005, **72**, 132103.
112 Y. Akahama, H. Kawamura, S. Carlson, T. Le Bihan and D. Häusermann, *Phys. Rev. B: Condens. Matter Mater. Phys.*, 2000, **61**, 3139–3142.
113 J. C. Jamieson, *Science*, 1963, **140**, 72–73.
114 H. Xia, S. J. Duclos, A. L. Ruoff and Y. K. Vohra, *Phys. Rev. Lett.*, 1990, **64**, 204–207.
115 Y. Akahama, H. Kawamura and T. Le Bihan, *J. Phys.: Condens. Matter*, 2002, **14**, 10583–10588.
116 R. Ahuja, L. Dubrovinsky, N. Dubrovinskaia, J. M. Osorio Guillen, M. Mattesini and B. Johansson, *Phys. Rev. B: Condens. Matter Mater. Phys.*, 2004, **69**, 184102.
117 K. Takemura, in *Science and Technology at High Pressure*, Proceedings of AIRAPT-17, ed. M. H. Manghnani, W. J. Nellis and M. F. Nicol, 2000, Universities Press (India) Limited, Hyderabad, India, pp. 443–444 .
118 H. Cynn and C.-S. Yoo, *Phys. Rev. B: Condens. Matter Mater. Phys.*, 1999, **59**, 8526–8529.
119 L. C. Ming and M. H. Manghnani, *J. Appl. Phys.*, 1978, **49**, 208–212.
120 Y. K. Vohra and A. L. Ruoff, *Phys. Rev. B: Condens. Matter*, 1990, **42**, 8651–8654.
121 A. L. Ruoff, H. Xia, H. Luo and Y. K. Vohra, *Appl. Phys. Lett.*, 1990, **57**, 1007–1009.
122 H. Fujihisa and K. Takemura, *Phys. Rev. B: Condens. Matter*, 1995, **52**, 13257–13260.
123 P. W. Bridgman, *Proc. Am. Acad. Arts Sci.*, 1955, **84**, 111–129.
124 Y. K. Vohra, S. J. Duclos and A. L. Ruoff, *Phys. Rev. B: Condens. Matter*, 1987, **36**, 9790–9792.
125 Y. K. Vohra and A. L. Ruoff, *High Presure Res.*, 1990, **4**, 296–299.
126 J. C. Jamieson and A. W. Lawson, *J. Appl. Phys.*, 1962, **33**, 776–780.
127 T. Takahashi and W. A. Bassett, *Science*, 1964, **145**, 483–486.
128 H. K. Mao, W. A. Bassett and T. Takahashi, *J. Appl. Phys.*, 1967, **38**, 272–276.
129 H. K. Mao, Y. Wu, L. C. Chen, J. F. Shu and R. J. Hemley, *High Pressure Res.*, 1990, **5**, 773–775.
130 R. J. Hemley and H. K. Mao, *Int. Geology Rev.*, 2001, **43**, 1–30.

131 H. Cynn, J. E. Klepeis, C.-S. Yoo and D. A. Young, *Phys. Rev. Lett.*, 2002, **88**, 135701.
132 F. Occelli, D. L. Farber, J. Badro, C. M. Aracne, D. M. Teter, M. Hanfland, B. Canny and B. Couzinet, *Phys. Rev. Lett.*, 2004, **93**, 095502.
133 C. S. Yoo, H. Cynn, P. Söderlind and V. Iota, *Phys. Rev. Lett.*, 2000, **84**, 4132–4135.
134 E. A. Perez-Albuerne, K. F. Forsgren and H. G. Drickamer, *Rev. Sci. Instrum.*, 1964, **35**, 29–33.
135 Y. Cerenius and L. Dubrovinsky, *J. Alloys Compd.*, 2000, **306**, 26–29.
136 H. K. Mao, P. M. Bell, J. Shaner and D. J. Steinberg, *J. Appl. Phys.*, 1978, **49**, 3276–3283.
137 P. M. Bell, J. Xu and H. K. Mao, in *Shock Waves in Condensed Matter*, ed. Y. M Gupta, Plenum, New York, 1986.
138 K. Takemura, *Phys. Rev. B: Condens. Matter*, 1997, **56**, 5170–5179.
139 R. W. Lynch and H. G. Drickamer, *J. Phys. Chem. Solids*, 1965, **26**, 63.
140 K. Takemura, *Phys. Rev. Lett.*, 1995, **75**, 1807–1810.
141 W. Potzel, M. Steiner, H. Karzel, W. Schiessl, M. Köfferlein, G. M. Kalvius and P. Blaha, *Phys. Rev. Lett.*, 1995, **74**, 1139–1142.
142 O. Schulte and W. B. Holzapfel, *Phys. Rev. B: Condens. Matter*, 1996, **53**, 568–580.
143 K. Takemura, *Phys. Rev. B: Condens. Matter Mater. Phys.*, 1999, **60**, 6171–6174.
144 K. Takemura, H. Yamawaki, H. Fujihisa and T. Kikegawa, *Phys. Rev. B: Condens. Matter Mater. Phys.*, 2002, **65**, 132107.
145 W. Klement, Jr., A. Jayaraman and G. C. Kennedy, *Phys. Rev.*, 1963, **131**, 1–6.
146 O. Schulte and W. B. Holzapfel, *Phys. Lett. A*, 1988, **131**, 38–40.
147 R. G. Green, H. Luo and A. L. Ruoff, *Phys. Rev. Lett.*, 1994, **73**, 2075–2078.
148 Y. Akahama, M. Nishimura, K. Kinoshita, H. Kawamura and Y. Ohishi, *Phys. Rev. Lett.*, 2006, **96**, 045505.
149 P. W. Bridgman, *Phys. Rev.*, 1935, **48**, 893–906.
150 A. Jayaraman, W. Klement, R. C. Newton and G. C. Kennedy, *J. Phys. Chem. Solids*, 1963, **24**, 7–18.
151 O. Schulte and W. B. Holzapfel, *Phys. Rev. B: Condens. Matter*, 1997, **55**, 8122–8128.
152 T. Kenichi, K. Kazuaki and A. Masao, *Phys. Rev. B: Condens. Matter Mater. Phys.*, 1998, **58**, 2482–2486.
153 K. Takemura, *Phys. Rev. B: Condens. Matter*, 1991, **44**, 545–549.
154 O. Schulte, A. Nikolaenko and W. B. Holzapfel, *High Pressure Res.*, 1991, **6**, 169–182.
155 G. J. Piermarini and C. E. Weir, *J. Res. Natl. Bur. Stand. (U. S.)*, 1962, **66A**, 325–333.
156 M. Liu and L. Liu, *High Temp.-High Pressures*, 1986, **18**, 79.
157 H. Olijnyk and W. B. Holzapfel, *J. de Phys. C*, 1984, **8**, 153–156.
158 S. Desgreniers, Y. K. Vohra and A. L. Ruoff, *Phys. Rev. B: Condens. Matter*, 1989, **39**, 10359–10361.
159 T. Takahashi, H. K. Mao and W. A. Bassett, *Science*, 1969, **165**, 1352–1353.
160 C. A. Vanderborgh, Y. K. Vohra, H. Xia and A. L. Ruoff, *Phys. Rev. B: Condens. Matter*, 1990, **41**, 7338–7340.
161 M. I. McMahon, O. Degtyareva and R. J. Nelmes, *Phys. Rev. Lett.*, 2000, **85**, 4896–4899.
162 Y. Akahama, H. Kawamura and A. K. Singh, *J. Appl. Phys.*, 2002, **92**, 5892–5897.
163 M. I. McMahon and R. J. Nelmes, *Z. Kristallogr.*, 2004, **219**, 742–748.
164 K. Aoki, S. Fujiwara and M. Kusakabe, *Solid State Commun.*, 1983, **45**, 161–163.
165 T. Kikegawa and H. Iwasaki, *J. Phys. Soc. Jpn.*, 1987, **56**, 3417–3420.
166 H. J. Beister, K. Strössner and K. Syassen, *Phys. Rev. B: Condens. Matter*, 1990, **41**, 5535–5543.
167 R. G. Greene, H. Luo and A. L. Ruoff, *Phys. Rev. B: Condens. Matter*, 1995, **51**, 597–600.
168 H. Luo, S. Desgreniers, Y. K. Vohra and A. L. Ruoff, *Phys. Rev. Lett.*, 1991, **67**, 2998–3001.
169 K. Aoki, O. Shimomura and S. Minomura, *J. Phys. Soc. Jpn.*, 1980, **48**, 551–556.
170 G. Parthasarathy and W. B. Holzapfel, *Phys. Rev. B: Condens. Matter*, 1988, **37**, 8499–8501.
171 Y. Omasa, I. Yamamoto, M. Yao and H. Endo, *J. Phys. Soc. Jpn.*, 1995, **64**, 4766–4789.
172 H. Luo and A. L. Ruoff, *Phys. Rev. B: Condens. Matter*, 1993, **48**, 569–572.
173 H. Luo, R. G. Greene and A. L. Ruoff, *Phys. Rev. Lett.*, 1993, **71**, 2943–2946.
174 H. Fujihisa, Y. Akahama, H. Kawamura, H. Yamawaki, M. Sakashita, T. Yamada, K. Honda and T. Le Bihan, *Phys. Rev. B: Condens. Matter Mater. Phys.*, 2004, **70**, 134106.
175 O. Degtyareva, E. Gregoryanz, M. Somayazulu, P. Dera, H. K. Mao and R. J. Hemley, *Nat. Mater.*, 2005, **4**, 152–155.
176 Y. Akahama, M. Kobayashi and H. Kawamura, *Phys. Rev. B: Condens. Matter*, 1993, **48**, 6862–6864.
177 C. Hejny, L. F. Lundegaard, S. Falconi, M. I. McMahon and M. Hanfland, *Phys. Rev. B: Condens. Matter Mater. Phys.*, 2005, **71**, 020101(R).
178 F. J. H. Etters and N. E. Christensen, *Phys. Rev. B: Condens. Matter Mater. Phys.*, 2004, **69**, 214112.
179 T. Ishikawa, H. Nagara, K. Kusakabe and N. Suzuki, *Phys. Rev. Lett.*, 2006, **96**, 095502.
180 S. K. Reed and G. J. Ackland, *Phys. Rev. Lett.*, 2000, **84**, 5580–5583.
181 U. Haüssermann, K. Söderburg and R. Norrestam, *J. Am. Chem. Soc.*, 2002, **124**, 15359–15367.
182 A. Ormeci and H. Rosner, *Z. Kristallogr.*, 2004, **219**, 370–375.
183 O. Degtyareva, R. Caracas, E. Gregoryanz, R. Cohen, H. K. Mao and R. J. Hemley, *Acta Crystallogr., Sect. A: Fundam. Crystallogr.*, 2005, **61**, C467.
184 V. F. Degtyareva, in *High-Pressure Crystallography*, ed. A. Katrusiak and P. F. McMillan, Kluwer Academic Publishers, Dordrecht, 2004, pp. 447–456.
185 G. J. Ackland and I. D. Macleod, *New J. Phys.*, 2004, **6**, 138.
186 H. Katzke and P. Tolédano, *Phys. Rev. B: Condens. Matter Mater. Phys.*, 2005, **71**, 184101.
187 J. S. Tse, *Z. Kristallogr.*, 2005, **220**, 521–530.
188 L. J. Parker, T. Atou and J. V. Badding, *Science*, 1996, **273**, 95–97.
189 M. Hasegawa, T. Atou and J. V. Badding, *J. Solid State Chem.*, 1997, **130**, 311–315.
190 T. S. Snider and J. V. Badding, *Solid State Commun.*, 2004, **131**, 157–161.